The influence of multi-walled carbon nanotubes on single-phase heat transfer and pressure drop characteristics in the transitional flow regime of smooth tubes

J.P. Meyer[*], T.J. McKrell[**], K. Grote

Department of Mechanical and Aeronautical Engineering, University of Pretoria, Pretoria Private Bag X20, Hatfield 0028, South Africa.

[**]*Massachusetts Institute of Technology, 77 Massachusetts Avenue, Cambridge, MA 02139-4307, USA.*

Abstract

In this paper, the convective heat transfer enhancement of aqueous suspensions of multi-walled carbon nanotubes flowing through a straight horizontal tube was investigated experimentally for a Reynolds number range of 1 000 - 8 000, which included the transitional flow regime. The tube was made out of copper with an internal diameter of 5.16 mm. Experiments were conducted at a constant heat flux of 13 kW/m^2 with 0.33%, 0.75% and 1.0% volume concentrations of multi-walled carbon nanotubes. The nanotubes had an outside diameter of 10 - 20 nm, an inside diameter of 3 - 5 nm and a length of 10 - 30 µm. Temperature and pressure drop measurements were taken, from which the heat transfer coefficients and friction factors were determined as a function of Reynolds number. It was found that heat transfer was enhanced when comparing the data on a Reynolds-Nusselt graph but when comparing the data at the same velocity, it was shown that heat transfer was not enhanced. Performance evaluation of the nanofluids showed that the increase in viscosity was four times the increase in the thermal conductivity, which resulted in an inefficient nanofluid.

Keywords: Nanofluids, multi-walled carbon nanotubes, transition, convective heat transfer, performance evaluation

* Corresponding author.
E-mail address: josua.meyer@up.ac.za (J.P. Meyer)

Nomenclature

As	Surface area, m^2
C	Constant
c_p	Specific heat at constant pressure, J/kg K
D	Internal diameter of tube, m
EB	Energy balance
ΔP	Pressure drop across the tube, Pa
f	Darcy-Weisbach friction factor
h	Convective heat transfer coefficient, W/m^2 ˚C
$h(x)$	Local convective heat transfer coefficient, W/m^2 ˚C
I	Current, A
k	Thermal conductivity, W/m ˚C
L	Length of tube, m
$\dot{m}$	Mass flow rate, kg/s
n	Number of temperature measuring points
P	Perimeter of tube, m
$\dot{Q}_{in}$	Heat input from heater, W
$\dot{Q}_{tf}$	Heat transfer to the test fluid, W
$\dot{q}$	Heat flux, W/m^2
R	Thermal resistance, ˚C/W
T	Temperature, ˚C
$T(x)$	Local temperature, ˚C
V	Velocity, m/s
V	Voltage, V
x	Axial distance, m

Greek Symbols

δ_t	Thermal boundary layer thickness, m
μ	Dynamic viscosity, kg/m s
ϕ	Volume concentration
ρ	Density, kg/m^3

Non-dimensional Numbers

Gr	Grashof number
Gz	Graetz number
Nu	Nusselt number
Pr	Prandtl number
Ra	Rayleigh number ($Ra = Gr \cdot Pr$)
Re	Reynolds number

Subscripts

avg	Average
b	Bulk
bf	Base fluid
Cu	Copper
e	Exit
in	Input
i	Inlet
k	Thermal conductivity
lam	Laminar
m	Mean
nf	Nanofluid

p	Particle
si	Inner surface
so	Outer surface
tf	Testing fluid
trans	Transition
turb	Turbulent
w	Wall
x	Local properties
μ	Viscosity

1. Introduction

There is an exponential growth in communication, electronics and computing technologies. Together with a steady decrease in their size and an enhanced rate of operation and storage of data, challenges arise in their thermal management. The conventional method is to increase the cooling rate by increasing the heat transfer surface area, but this approach requires an undesirable increase of the thermal management system [1]. On a large scale, such as power generation, chemical production, air-conditioning and transportation, one requires more efficient cooling systems with greater cooling capacities and a decreased size [2,3]. Research is being done on microscale heat transfer; however, the conventional fin-and-microchannel technology appears to be inadequate for next generation technologies [2].

The low heat transfer performance of conventional fluids such as water, engine oil and ethylene glycol hinders the performance enhancement and the compactness of heat exchangers [1,4,5]. The thermal conductivity of a fluid plays a vital role in the development of energy-efficient heat transfer equipment but they have an order-of-magnitude smaller

thermal conductivity than metallic or non-metallic particulates. When comparing the thermal conductivity of water (0.61 W/m˚C) with that of multi-walled carbon nanotubes (MWCNT), the thermal conductivity of the carbon nanotubes (3 000 W/m˚C) is about 5 000 times larger than that of water. By the introduction of nanometre sized solid particles, the thermal conductivity of the fluid is improved thereby improving its capability of energy exchange. These fluids are termed "nanofluids" and are deemed the next generation heat transfer fluid.

Pak and Cho [6] did experiments with γ-Al_2O_3-water and TiO_2-water nanofluids for fully turbulent flow and got a 45% enhancement in the heat transfer coefficient with the γ-Al_2O_3-water nanofluid at a volume concentration of 1.34% and for the TiO_2-water nanofluid, a 75% enhancement in the heat transfer coefficient at a volume concentration of 2.78%. But at the same concentration, the heat transfer enhancement for the TiO_2-water nanofluid was less than that of the γ-Al_2O_3-water nanofluid.

Li and Xuan [7] used a Cu-water nanofluid in their experiments and tested in the laminar and turbulent flow regimes. Compared with water, the convective heat transfer coefficient of the nanofluid was increased by about 60% for a volume concentration of 2% for the same Reynolds number.

Wen and Ding [8] performed experiments at the entrance region under laminar flow condition using γ-Al_2O_3-water nanofluids. For a volume concentration of 1.6%, the local heat transfer coefficient was around 45% higher than that of water only. This enhancement decreased to around 14% further away from the entrance.

Yang *et al.* [9] did experiments with graphite-water nanofluids under laminar flow conditions. For a 2.5 wt% they experienced an increase in heat transfer of 22% over the base fluid at a temperature of 50°C and 15% at a temperature of 70°C.

Ding *et al.* [3] tested MWCNT-water nanofluids in the entrance region of laminar flow. They experienced a maximum enhancement in heat transfer of over 350% at a

Reynolds number of 800 and an axial distance of approximately 110 times the tube diameter for 0.5 wt% of MWCNTs.

Heris *et al.* [10] tested Al_2O_3-water nanofluids under laminar flow range conditions. They had heat transfer enhancement and found that as the particle volume concentration increases so does the enhancement. They tested volume concentrations of 0.2 vol% up to 2.5 vol%.

Murshed *et al.* [11] did experiments with TiO_2-water nanofluids under laminar flow conditions. They found for a volume concentration of 0.8 vol% and at position x/D = 25 that the local heat transfer coefficient of the nanofluid was about 12% and 14% higher than deionised water at a Reynolds number of 1 100 and 1 700 respectively.

Garg *et al.* [12] also tested MWCNT-water nanofluids. Their experiment was concerned about the preparation and the enhancement in the laminar flow range using MWCNT-water nanofluids. They had a maximum heat transfer enhancement of 32% at a Reynolds number of 600.

Kim *et al.* [13] used two different nanofluids in their experiments. They tested in the laminar and turbulent flow range. The two nanofluids they used were γ-Al_2O_3-water and amorphous carbonic water. In laminar flow the γ-Al_2O_3-water nanofluids had a heat transfer enhancement of around 14% whereas the amorphous carbonic nanofluid showed enhancement of around 7%. In turbulent flow, the γ-Al_2O_3-water nanofluids had an increase of around 20% and the amorphous carbonic water nanofluid showed no enhancement.

Anoop *et al.* [14] did experiments with γ-Al_2O_3-water nanofluids with different particle sizes in the laminar flow range. They showed that there is larger heat transfer enhancement with a smaller particle size than a larger one. At a Reynolds number of 1 550 for the 45 nm particle size, the enhancement was around 25% whereas for a 150 nm particle size the enhancement was 11%.

Amrollahi *et al.* [15] did experiments with functionalized MWCNT-water in laminar and turbulent flow at the entrance region. Under laminar flow the heat transfer coefficient is increased by 25% for a concentration of 0.12 wt% at 20°C. In the turbulent flow regime the heat transfer enhancement increases between 5-25% for different temperatures and particle concentrations.

Liu and Liao [16] tested CNT's suspended in an aqueous drag-reducing fluid for the turbulent flow range. At high temperatures the heat transfer enhancement for 1.0 wt% increases by about 40% compared to that of water.

Duangthongsuk and Wongwises [17] tested TiO_2-water nanofluids for the turbulent flow range. At a volume concentration of 1%, the heat transfer enhancement was approximately 26% whereas at a volume concentration of 2%, the heat transfer enhancement was reduced by 14%.

Ferrouillat *et al.* [18] tested SiO_2-water nanofluids for the entire flow range but only considered results for the turbulent flow range. At a volume concentration of 18.9%, the heat transfer enhancement was approximately 50% for a Reynolds number greater than 1 000.

Table 1 summarises the previous work found in literature. It shows which flow range was tested in, what type of nanofluid was used and the percentage enhancement in heat transfer over that of the base fluid water.

Evaluating the literature shows that there are few works [6,7,8,9,10,11,13,14,17,18] that have reported on convective heat transfer characteristics of nanofluids, especially CNT nanofluids [3,12,15,16]. All of the studies considered in literature either test in the laminar [3,7,8,9,10,11,12,13,14,15] or high turbulent flow range [6,7,13,15,16,17] and very few tested in the transitional flow range [19].

It is normally advised when designing heat transfer equipment to remain outside the transitional flow regime due to the uncertainty and flow instability of this region. Large

pressure variations are also encountered in this region since the pressure gradient required to pump the fluid in laminar and turbulent flow could vary by an order of magnitude. As more and more sophisticated heat transfer enhancement techniques are being used in heat exchangers, the mass flow rates have slowly decreased over the years for a specific heat transfer rate and these days a lot of heat transfer equipment has started operating close to or in the transitional flow range. Thus there is a need for more design information in transitional flow. In the recent works of Meyer and Olivier [20,21,22], the heat transfer coefficients and pressure drops were measured for transitional flow in smooth and enhanced tubes with different types of inlets. They showed that the heat transfer and pressure drop characteristics are stable and that there is a smooth transition from laminar to turbulent flow. They also showed that if heat transfer occurs, the type of inlet has no influence on the heat transfer coefficients, friction factors and on the critical Reynolds number.

No work has thus far been conducted to investigate the influence of MWCNTs on single-phase heat transfer and pressure drop characteristics in the transitional flow regime of smooth tubes. Therefore, the purpose of this study is to experimentally measure, for a few low concentrations of MWCNTs suspended in water, the heat transfer and pressure drop characteristics of nanofluids in the laminar, transitional and turbulent flow regime in a horizontal smooth tube.

Hence the separate objectives of this study will, firstly, be to obtain heat transfer coefficient and friction factor data for Reynolds numbers between 1 000 and 8 000 (this is done to include the transition point where the flow changes from laminar to turbulent), for smooth tubes using water and three different concentrations of MWCNT-water nanofluids as the working fluid. The second objective will be to evaluate the performance of MWCNT-water nanofluids as a heat transfer enhancement fluid.

2. Experimental set-up and validation

2.1. Nanofluid preparation

Three different volume concentrations, measured according to the volume of the base fluid, of MWCNT-water nanofluids were prepared. The MWCNTs have an outside diameter of 10 - 20 nm, an inside diameter of 3 - 5 nm and a length of 10 - 30 μm. The three different volume concentrations were 0.33%, 0.75% and 1.0%, which were dispersed into 10 *litres* of distilled water. In order to stabilise the three different mixtures, gum arabic (GA) powder was dissolved and added into the distilled water first. Garg *et al.* [12] used 0.25 wt% GA with 1 wt% MWCNT, or a 1:4 ratio. A similar approach was used here. Garg *et al.* [12] sonicated various nanofluid samples for different time lengths. They found that the optimum sonication time for a 1 wt% MWCNT and 0.25 wt% GA mixture was 40 min using a 130 W, 20 kHz ultrasonicator. In the current study, the nanofluids were sonicated using an ultrasonicator that had an operating frequency of 24 kHz and a maximum power output of 200 W. The sonication times for the current nanofluids were adjusted to match the optimum sonication time of Garg *et al.* [12]. Hence the sonication times for the volume concentrations of 0.33%, 0.75% and 1.0% were 30 min, 80 min and 120 min respectively.

For a stable nanoparticle-dispersion, the pH is a key parameter, which is related to the electrostatic charge on the particles' surface and is known as the zeta potential. At the iso-electric point, which is the point where the nanoparticle carries no net electrical charge, the nanoparticles will form agglomerations since there are no sufficient repulsive forces between the nanoparticles. As the pH changes from the iso-electric point, the absolute value of the zeta potential of the nanoparticle surface increases so that agglomeration and collisions between nanoparticles caused by Brownian motion are prevented [23]. Shown in Figure 1 is the measured pH of the distilled water compared with that of the MWCNT-water nanofluid and GA-water mixture. The pH of the distilled water is 7.1 and that of the GA-water mixture

for volume concentrations of 0.33%, 0.75% and 1.0% is 6.6, 6.4 and 7.4 respectively. The MWCNT-water nanofluids follow a similar trend as that of the GA-water mixture except at a concentration of 1.0 vol%, the suspension is not acidic. At volume concentration of 0.33%, 0.75% and 1.0% the pH is 8.0, 7.7 and 7.1 respectively. Xie *et al.* [24] found that the iso-electric point of their MWCNT suspension was at a pH of 7.3. The 0.33 vol% and 0.75 vol% nanofluid concentrations remained stable for 3 days whereas the 1.0 vol% only remaind stable for around 24 hours due to the large possibility of its nanoparticles forming agglomerations and settling out of the suspension.

2.2. Effective thermal conductivity of the MWCNT-water nanofluid

The thermal conductivity was measured using a KD2 thermal property meter (Decagon Devices), which is based on the transient line heat source method. The KD2 thermal property meter had a measurement uncertainty of ±5% and was calibrated by using distilled water before any set of measurements were taken. The results fall to within 5% of the predicted theory by Popiel and Wojtkowiak [25].

Shown in Figure 2 is the measured thermal conductivity ratio of the 0.33 vol%, 0.75 vol% and 1.0 vol% MWCNT-water nanofluids for a temperature range of 20˚C - 40˚C. The effective thermal conductivity increases with increasing temperature and MWCNT concentration. For volume concentrations of 0.33%, 0.75% and 1.0%, the thermal conductivities of the MWCNT-water nanofluids were 2%, 3.3% and 8% respectively greater than that of the distilled water. The results show that the increase in thermal conductivity falls to within the measurement uncertainty of the device. The reason is that the thermal conductivity meter is very sensitive to natural convection. At 20°C the data follows almost a straight line. This is due to that fact that natural convection in the sample is low. The scatter in the data increases with increasing temperature.

Xie *et al.* [24] reported a 7% increase in thermal conductivity for MWCNT suspended in water at a volume concentration of 1.0%, which compares very well with the measured 8%. Prasher *et al.* [26] showed that the thermal conductivity can increase due to agglomeration of the nanoparticles when compared with a well-dispersed system, which is a possible reason for the large increase in the thermal conductivity of the 1.0 vol% MWCNT-water nanofluid. Keblinski *et al.* [27] also showed that particle clustering, due to Brownian motion, could enhance the thermal conductivity since the particles are much closer together and thus enhance the constant phonon heat transfer.

Prasher *et al.* [28] showed that the thermal conductivity can be written as follows:

$$\frac{k_{nf}}{k_{bf}} = 1 + C_k \cdot \phi \qquad (1)$$

where C_k is a constant depending on the experimental data. In this case, $C_k = 7$ and is shown in Figure 2 as the dotted black line. On average, Equation 1 predicts the thermal conductivity to within 1.8% for all three volume concentrations.

2.3. Effective viscosity of the MWCNT-water nanofluid

When plotting the results on a viscosity vs. temperature graph the viscosity of nanofluids increases with increasing MWCNT concentration and decreasing temperature. Figure 3 shows the measured viscosity ratios as a function of the volume concentrations of the MWCNT-water nanofluids. When plotting the results in this fashion the different temperature data points collapse onto one point and the viscosity-ratio is then only dependent on the volume concentration.

The viscosities were measured with a double concentric cylinder viscosity meter. There is a linear increase from a volume concentration of 0% up to 0.75% and then suddenly a steep increase to 1.0%. A possible reason for the large increase in viscosity is that the nanoparticles have agglomerated due to the pH of the solution being too close to the iso-electric point [23].

Einstein, in 1906, developed a correlation for the viscosity of dilute suspensions (< 5 vol%) for small and rigid spherical particles [29]:

$$\frac{\mu_{nf}}{\mu_{bf}} = 1 + 2.5 \cdot \phi \qquad (2)$$

Equation 2 is shown as the blue line on Figure 3. Equation 2 under predicts the data for the 0.33 vol% MWCNT-water nanofluid concentration by 15.9%, for the 0.75 vol% MWCNT-water nanofluid concentration by 29.7% and for the 1.0 vol% MWCNT-water nanofluid concentration by 77.7%. The reason for the large under prediction by Equation 2 is that the correlation was developed for spherical particles. Equation 2 can be extended to include ellipsoidal particles [18,28]:

$$\frac{\mu_{nf}}{\mu_{bf}} = 1 + \mathrm{C_\mu} \cdot \phi \qquad (3)$$

where C_μ depends on the ratio of the revolution ellipsoid axes and is equal to 2.5 for spherical particles and not tubes with an aspect ratio of 1 333. In this case, C_μ equal to 60 correlates the volume concentrations of 0.33% and 0.75% well. At a volume concentration of 0.33%, Equation 3 over predicts the viscosity by 0.24%, at a volume concentration of 0.75%, the viscosity is under predicted by 0.17% and at a volume concentration of 1.0%, the viscosity is under predicted by 65.1%.

2.4. Experimental set-up

Shown in Figure 4 was the experimental set-up used. An electronically controlled magnetic gear pump (*Item* 1) was used to pump the working fluid at a stable flow rate. A bypass loop, which was controlled via a gate valve (*Item* 11), was added to control the flow rate. In order to protect the equipment, a pressure relief valve (*Item* 2), which was rated at 350 kPa, and a non-return valve (*Item* 3) were incorporated into the system. The inlet and exit thermocouples (*Item* Ti and Te respectively) were attached to the system to measure the inlet and outlet temperatures, rather than the test section, since this will avoid any influence that the test section has on the readings. The test section (*Item* 5) is connected to the system via rubber hosing, so as to prevent axial conduction. The flow rate through the test section was measured via a Coriolis flow meter (*Item* 6), which was placed after the test section. After the flow meter, the fluid is cooled back to the inlet temperature (≈ 20°C) via the cooling loop, which consists of a simple tube-in-tube heat exchanger (*Item* 7), chiller (*Item* 8) and a centrifugal pump (*Item* 9), before it is pumped back to the 22 *litre* storage tank (*Item* 10). Just after and before the storage there are three ball valves (*Item* 4) which allow the system to be flushed and cleaned easily. The system and storage tank were kept small to ensure that the volume MWCNT (which is very expensive) used was kept to a minimum.

Shown in Figure 5 is the test section used in the current study. The test section consisted of a 500 mm hydrodynamic entry section, a heat transfer test section and a mixer, and all three sections were separated from each other by acetyl bushes. The acetyl bushes were used to thermally insulate the mixer and inlet sections from the heat transfer test section. The heat transfer test section consisted of a straight copper tube of length 1 m. It had an internal diameter of 5.16 mm and an external diameter of 6.44 mm. The test section was insulated with 60 mm thick insulation. The heat transfer test section was heated via a Constantine wire at 212 W (13 000 W/m^2) with a DC power supply at 200 V and a current of

1.06 A. To measure the wall temperatures, 13 T-type thermocouples were spaced evenly along the test section wall. This was done by drilling a small pilot hole into the test section and securing the thermocouple with a drop of solder. Two T-type thermocouples were inserted into the fluid, before the developing length and after the mixer, in order to measure the inlet and outlet temperatures. The thermocouples were calibrated to an accuracy of 0.1˚C. The pressure drops were measured with a pressure transducer with an accuracy of 0.08% at full scale, which was 17 kPa. The pressure range of the experiments was from 155 Pa to 8.2 kPa. The pressure transducer was connected to the pressure taps shown in Figure 5. The pressure tap diameter was 4 mm, which is less than 10% of the tube diameter. The reason for the small diameter is so that the overall flow is not disturbed since a large hole could lead to a localised eddy forming which results in an error in pressure readings [20,21]. The flow rate was measured using a Coriolis flow meter, which had an accuracy of 0.05% at full scale.

2.5. Data reduction

The local convective heat transfer coefficient, $h(x)$, was calculated as:

$$h(x) = \frac{\dot{q}_{in}}{T_{si}(x) - T_m(x)} \quad (4)$$

The heat flux, $\dot{q}_{in}$, was determined from the electrical energy input, $\dot{Q}_{in} = V \cdot I$, and the inner surface area, $A_s = \pi \cdot D \cdot L$. The electrical energy input remained constant at 212 W throughout the measurements thus resulting in a constant heat flux (≈ 13 kW/m^2).

The inner local surface temperature, $T_{si}(x)$, was determined from the measurements of the outside wall temperature, T_{so}, and the heat transfer and resistance through the tube wall:

$$T_{si}(x) = T_{so}(x) - \dot{Q}_{in} \cdot R_w \quad (5)$$

where

$$R_w = \frac{\ln(D_{so}/D_{si})}{2 \cdot \pi \cdot k_{Cu} \cdot L} \quad (6)$$

The thermal conductivity of the copper was obtained from Abu-Eishah [30] and is given by

$$k_{Cu} = a \cdot T_{Cu}^{b} \cdot e^{c \cdot T_{Cu} + d/T_{Cu}} \quad (7)$$

where the constants a = 82.56648, b = 0.262301, c = $-4.06701 \cdot 10^{-4}$ and d = 59.72934. T_{Cu} is the mean temperature of the copper tube in Kelvins.

The local heat transfer coefficient was determined from the local mean temperature. The local mean temperature was determined by [31]:

$$T_m(x) = T_i + \frac{\dot{q}_{in} \cdot x \cdot P}{\dot{m} \cdot c_p} \quad (8)$$

To obtain the average heat transfer coefficient, Equation 4 was averaged along the length of the tube at different measuring points, n. This was done by taking the mean of all the local heat transfer coefficients.

$$h_{avg} = \frac{h(x_1) + \cdots + h(x_n)}{n} \quad (9)$$

The average Nusselt number can then be calculated as follows:

$$Nu_{avg} = \frac{h_{avg} \cdot D}{k} \quad (10)$$

where k is the thermal conductivity of the working fluid, determined at the bulk fluid temperature, $T_b = (T_i + T_e)/2$, For water the thermal conductivity was determined from the equations developed by Popiel and Wojtkowaik [25].

The testing fluids average Reynolds number and Prandtl number,

$$Re = \frac{4 \cdot \dot{m}}{\pi \cdot D \cdot \mu} \quad (11)$$

$$Pr = \frac{\mu \cdot c_p}{k} \quad (12)$$

were calculated based on the viscosity, thermal conductivity and specific heat determined at the bulk fluid temperature, T_b, using the equations developed by Popiel and Wojtkowaik [25] for water and for the MWCNT nanofluid the measured values of its properties were used.

The pressure loss equation is used to calculate the friction factor:

$$f = \frac{\Delta P \cdot D \cdot 2}{L \cdot \rho \cdot V_{avg}^2} \quad (13)$$

which was then simplified to:

$$f = \frac{\Delta P \cdot \rho \cdot \pi^2 \cdot D^5}{8 \cdot L \cdot \dot{m}^2} \quad (14)$$

The pressure drop was determined from the pressure drop measurements of the transducer and the mass flow rate was determined from the readings of the Coriolis mass flow meter.

The measured heat transfer of the testing fluid was compared with that of the electrical input energy, $\dot{Q}_{in}$, which was supplied by the Constantine heating wire, by means of an energy balance:

$$EB = \frac{\dot{Q}_{in} - \dot{Q}_{tf}}{(\dot{Q}_{in} + \dot{Q}_{tf})/2} \cdot 100 \quad (15)$$

where $\dot{Q}_{in}$ = 212 W and the heat transfer to the testing fluid, $\dot{Q}_{tf}$, is

$$\dot{Q}_{tf} = \dot{m} \cdot c_p \cdot (T_e - T_i) \quad (16)$$

Although energy balances of around 3% were obtained, the input energy was used for the calculations since it was the most accurate of the two.

2.6. Uncertainty

All uncertainties were calculated within the 95% confidence level using the method of Moffat [32]. Table 2 lists the instruments used in the study with their uncertainties. The uncertainty of the heat transfer coefficient is between 1.4% for the low Reynolds number (≈ 1 000) and up to 2.5% for the highest Reynolds number (≈ 8 000) tested. The friction factor has an uncertainty of 18% for the lowest Reynolds number and goes down to 2% for the highest. The lowest pressure drop recorded is 155 Pa hence the uncertainty of 18% at the low Reynolds number. The uncertainties of the measurements are shown in Table 3 for the low Reynolds number and highest Reynolds number.

2.7. Experimental procedure

After the start-up of the system, it was necessary to let the system settle for at least two hours in order to reach steady-state conditions. This was due to the thermal inertia of the system being relatively slow before it got to steady-state temperatures and mass flow rates. Once the system was steady, small changes were made in the flow rates in order to achieve the desired mass flow rates for data capturing.

Steady-state conditions were monitored visually, in that there were no observable changes in the temperatures, pressure drops, mass flow rates and energy balances. In the transition region, steady-state conditions were difficult to achieve due to the continuous fluctuations of temperatures, pressure drops and energy balances. But once the fluctuations repeated themselves periodically, measurements were taken. After the change in the mass flow rate from a high flow rate to low flow rate, it took approximately 5 - 10 min for steady-state conditions to be met. The reason for decreasing the flow rate was to ensure that very little residual heat was stored in the insulation, which has an effect on the next reading. On average, an energy balance of 3% was achieved before the data was captured. For each data point, 200 readings at a rate of 20 Hz were captured with a data acquisition system and then averaged for data reduction.

2.8. Validation

The heat transfer coefficients and friction factors were validated by taking measurements in the laminar and turbulent flow regimes and comparing these with published data. Adiabatic friction factors were used to validate the experiments since they disregard any influence of heat transfer on the properties. Diabatic friction factors were also measured and compared with published data. Only water was used to validate the experimental set-up as no other data exist for MWCNT-water nanofluids in a similar experimental set-up.

2.8.1. Adiabatic friction factors

The friction factor data consisted of 82 data points spanning a Reynolds number range of 1 000 - 8 000. Measurements were taken without any heat transfer to eliminate any varying density and viscosity effects. Figure 6 shows the adiabatic friction factor data as compared with Poiseuille flow ($f = 64/Re$) and the Blasius equation ($f = 0.3164 \cdot Re^{-0.25}$).

Comparing the laminar results with Poiseuille flow, the data is under predicted on average by 3.3% with a maximum deviation of 2.8%. For the turbulent data, the Blasius correlation under predicts the data, on average, by 0.2% with a maximum deviation of 0.5%. Generally, the friction factors in the laminar and turbulent flow regimes compare well with the Poiseuille and Blasius equations.

When considering the transitional flow regime, transition to turbulent flow appears to start at a Reynolds number of approximately 3 100 rather than the conventional value of 2 300 and the transitional flow range is also very short, around 100 Reynolds number long. The delayed transition and the sharp transition is the result of inlet effects as was shown by Olivier and Meyer [20] and by Meyer and Olivier [21].

2.8.2. Diabatic friction factors

Figure 7 shows the experimental data for the diabatic friction factor as a function of the Reynolds number compared with the laminar Poiseuille equation, the Blasius equation and corrected Blasius equation as suggested by Allen and Eckert [33]. Transition starts at a Reynolds number of approximately 2 900 and ends at a Reynolds number of approximately 3 600. The diabatic friction factors are lower than the adiabatic friction factors in laminar and turbulent flow. Allen and Eckert [33] proposed a viscosity correction factor, $(\mu_b \backslash \mu_w)^{-0.25}$, to be multiplied with the Blasius equation. The turbulent results correlate fairly well with the corrected Blasius equation (on average, the data is under predicted by 0.5% with a maximum

deviation of 1.9%). It should be noted that the correction factor is very close to unity (on average, it is 0.96) and the experimental data correlates with the Blasius equation, on average, by 1.9% with a maximum deviation of 2.1%.

In the laminar flow regime, the same phenomenon is observed as in the turbulent flow regime. Here the experimental data is under predicted by an average of 8.5% (however, it is within the uncertainties of 18% at low Reynolds numbers) with a maximum deviation of 2.2%. According to Shome and Jensen [34] and Tam and Ghajar [35], secondary flow effects increase the friction factor, especially in tubes with uniform heat flux boundary conditions. Tam and Ghajar [35] discovered that by increasing the overall heat flux, the laminar friction factors increased. The reason for this is that the wall-to-bulk temperature difference exists throughout the length of the tube [34].

Metais and Eckert [36] recommend the use of a flow map to distinguish between mixed and forced convection regimes. The map is based on the Reynolds number being a function of the Rayleigh number. Their flow map is for a constant wall boundary condition and hence cannot be used to compare the current data. Ghajar and Tam [37] developed a new flow map for a constant heat flux boundary condition. They used the data for three different inlets to produce a new boundary between laminar, transition and turbulent for both forced and mixed convection. Figure 8 shows the flow map developed by Ghajar and Tam [37] with the current data plotted. From the map, it can be concluded that experimental laminar values for this study are well within the laminar forced convection boundary and secondary flow effects are not present. Hence the reason for the drop in friction factor is the result of the reduction of liquid viscosity in the near-wall region due to heating [34], which seems to be the dominating effect.

2.8.3. Nusselt number

Heat transfer results were compared to the correlations developed by Ghajar and Tam [38] for laminar and turbulent flow, which are shown below:

$$Nu_{lam} = 1.24 \cdot [Gz + 0.025 \cdot (Gr \cdot Pr)^{0.75}]^{1/3} \cdot \left(\frac{\mu_b}{\mu_w}\right)^{0.14} \quad (17)$$

$$Nu_{turb} = 0.023 \cdot Re^{0.8} \cdot Pr^{0.385} \cdot \left(\frac{L}{D}\right)^{-0.0054} \cdot \left(\frac{\mu_b}{\mu_w}\right)^{0.14} \quad (18)$$

For the transitional flow regime, the correlation developed by Ghajar and Tam [38] was modified to account for a developing length inlet condition. The modified correlation is shown below:

$$Nu_{trans} = Nu_{lam} + \left[e^{\frac{Re_{trans}-Re}{36}} + Nu_{turb}^{-0.935}\right]^{-0.935} \quad (19)$$

The results are shown in Figure 9. In the laminar flow regime, the results are under predicted on average, by 5.2%, in the turbulent flow regime, on average, by 2.4% and in the transitional flow regime, on average, by 5.3%. Hence there was a good agreement between the equations by Ghajar and Tam [38] and the measurements over the Reynolds number range.

In general, the friction factors and Nusselt numbers in the laminar and turbulent flow regimes compare well with literature. This adds confidence in the measurement technique and further validates the experimental set-up and data reduction methodology.

2.9. Repeatability of results and stability of nanofluids

The results in Section 2.8 and in Section 3 were very repeatable. Many experiments were conducted over a few days and were repeated a few days later without any measureable

changes in results. The MWCNT-water nanofluid with volume concentrations of 0.33% and 0.75% remained stable for 3 days whereas the 1.0% nanofluid only remained stable for around 24 hours. However, after standing for more than 24 hours, the nanofluids were sonicated again before experiments were conducted.

Agglomeration of the nanoparticles was checked via a scanning electron microscope, but according to [29] it does not give a clear indication whether the particles have clustered together or not since during the drying process the particles cluster together. However, it was observed the particles had a fairly even distribution in the water. It was also observed that there was some entanglement of the particles especially for the 0.75 vol% and 1 vol% nanofluid but this could have been due to the preparation of the samples.

3. Results

3.1 Convective heat transfer of MWCNT-water nanofluids

MWCNT-water nanofluid concentrations of 0.33 vol%, 0.75 vol% and 1.0 vol% were tested for a Reynolds number range of 1 000 – 8 000. The results are shown in Figure 10 compared with the results of distilled water.

For fully turbulent flow, at a Reynolds number of typically 5 000, the heat transfer is enhanced by 9.7% when using the 0.33 vol% MWCNT-water nanofluid, by 23.5% when using the 0.75 vol% MWCNT-water nanofluid and by 33.2% when using the 1.0 vol% MWCNT-water nanofluid.

A possible reason for the increase in heat transfer is that the nanoparticles presented in the base liquid increase the thermal conductivity, delay and disturb the thermal boundary layer and accelerate the energy exchange process in the fluid due to the chaotic movement of the nanoparticles [13,17,39]. The increase in the thermal conductivity leads to an increase in heat transfer performance whereas the increase in viscosity leads to an increase in boundary

layer thickness, which results in a decrease in heat transfer performance [40]. Hence comparing heat transfer of a nanofluid to that of its base fluid at constant Reynolds number is generally not the best basis since the viscosity of the nanofluid is larger than that of its base fluid [6].

It was proposed by Pak and Cho [6] that a velocity comparison gives a more accurate representation of the heat transfer. Such a comparison is made in Figure 11. The results show that, at constant velocity, the heat transfer coefficient of the 0.33 vol% MWCNT-water nanofluid is 3.3% lower, at 0.75 vol%, it is 6.6% lower and at 1.0 vol%, it is 12.6% lower than that of distilled water. This trend of lower heat transfer coefficients in nanofluids compared with water was also experienced by Pak and Cho [6], Williams *et al.* [41] and Yu *et al.* [40]. However, at very high velocities, the heat transfer coefficients of the 0.33 vol% MWCNT-water nanofluid equal that of the distilled water. This could be due to the fact that nanofluids exhibit shear thinning behaviour at high shear rates [3,12,42], which decreases the viscosity and the nanofluid then enhances the heat transfer.

For transitional flow, the MWCNT-water nanofluid transition is delayed (see Figure 11) which is in agreement with the work by Liu and Yu [19]. This happens due to the particle-fluid interaction, which damps the instability and reduces the turbulence intensity and Reynolds stress in the flow.

The reason for the early transition when comparing the Nusselt number with the Reynolds number (see Figure 10) is that the viscosities of the MWCNT-water nanofluids are larger compared with those of distilled water, hence the results shift from the position shown in Figure 11 to the position shown in Figure 10 and due to the shift, the MWCNT-water nanofluids show enhancement in Nusselt numbers

For laminar flow, at a Reynolds number of 2 000, the heat transfer is reduced by 1.6% when using the 0.33 vol% MWCNT-water nanofluid, enhanced by 2.2% and 2.3% when using the 0.75 vol% and 1.0 vol% MWCNT-water nanofluid respectively.

A possible reason for the increase in the heat transfer coefficient for the MWCNT-water nanofluid at volume concentrations of 0.75% and 1.0%, and reduction in heat transfer coefficient for the MWCNT-water nanofluid at volume concentrations of 0.33%, can be explained by Figure 12. Shown in Figure 12 is the local heat transfer coefficient at various axial distances for MWCNT-water nanofluids, compared with distilled water at a Reynolds number of 2 000. Figure 12 shows that the MWCNT-water nanofluids, for volume concentrations of 0.75% and 1.0%, enhance the heat transfer up to an axial distance of approximately 120 tube diameters while the flow was developing. At 10 tube diameters, the 0.33 vol% MWCNT-water nanofluid heat transfer coefficient is less than that of the distilled water but between 25 and 90 tube diameters, the heat transfer coefficient is greater than that of the distilled water, after which it becomes less again than that of the distilled water. The heat transfer coefficient is directly proportional to k/δ_t. At the entrance, the thermal boundary layer thickness is zero and hence the heat transfer coefficient approaches infinity. The boundary layer thickness increases with axial distance until both the heat transfer coefficient and boundary layer thickness are constant. Hence an increase in the heat transfer coefficient results from either an increase in thermal conductivity or a decrease in the thermal boundary layer or both.

From Figure 12, it follows that the boundary layer thicknesses for the MWCNT-water nanofluids for volume concentrations of 0.75% and 1.0% are maximum at an axial distance of approximately 150 tube diameters. For the 0.33 vol% MWCNT-water nanofluid and distilled water, the maximum is at approximately 105 tube diameters. This results in a larger heat transfer coefficient for the 0.75 vol% and 1.0 vol% MWCNT-water nanofluids. After

105 tube diameters, both the distilled water and the 0.33 vol% MWCNT-water nanofluid heat transfer coefficients increase slightly, a 10% and 6% increase respectively. The possible reason for the dip in the local heat transfer coefficient could be due to an imposed bellmouth inlet. In such cases, the boundary layer along the tube wall is at first laminar and then changes through a transition region to the turbulent condition, causing a dip in the *h-x/D* curve. The length of the dip decreases with the increase of the turbulent Reynolds number [43]. At low particle concentrations, the dip is still present but it seems to reduce with an increase in the particle concentration, indicating that the presence of particles suppresses the effect of the bellmouth inlet.

3.2 Comparison of results with existing heat transfer correlations

Due to the increase in viscosity the MWCNT-water nanofluid results shifted to lower Reynolds numbers (see Figure 10), therefore the results were compared to correlations developed for water by substituting the nanofluid properties for the water properties. Comparing nanofluid results with developed correlations for water was also done by Yu *et al.* [40], Williams *et al.* [41] and Liu and Liao [16]. The properties of the nanofluids, such as the thermal conductivity and viscosity were determined from Equation 2 and 3. The density was determined from [6]:

$$\rho_{nf} = \phi \cdot \rho_p + (1 - \phi) \cdot \rho_{bf} \qquad (20)$$

The specific heat was determined from [19]:

$$(c_p)_{nf} = \frac{\phi \cdot \left(\rho \cdot c_p\right)_p + (1 - \phi) \cdot \left(\rho \cdot c_p\right)_{bf}}{\rho_{nf}} \qquad (21)$$

The correlation by Ghajar and Tam [38] was used for comparison purposes in the laminar and turbulent flow regime and Equation 19 was used for comparison purposes in the transitional flow regime. Figure 13 to Figure 15 show how the adjusted water correlations predict the MWCNT-water nanofluid results.

3.2.1 Heat transfer in the laminar flow regime

Shown in Figure 13 is the ratio of the predicted (Equation 17) to measured Nusselt numbers as a function of the laminar Reynolds numbers. The results for all three volume concentrations of MWCNT-water nanofluids are predicted to within 10%. For the 0.33 vol% MWCNT-water nanofluid, the data is over predicted by 1.8% with a maximum deviation of 4%, the 0.75 vol% MWCNT-water nanofluid is over predicted by 3.5% with a maximum deviation of 1.8% and the 1.0 vol% MWCNT-water nanofluid is over predicted by 8.6% with a maximum deviation of 2.4%.

3.2.2 Heat transfer in the turbulent flow regime

Shown in Figure 14 is the ratio of the predicted (Equation 18) to measured Nusselt numbers as a function of the turbulent Reynolds numbers. The results for all three volume concentrations of MWCNT-water nanofluids are predicted to within 10%. For the 0.33 vol% MWCNT-water nanofluid, the data is under predicted by 3.8% with a maximum deviation of 1.9%, the 0.75 vol% MWCNT-water nanofluid is under predicted by 5.8% with a maximum deviation of 2.2% and the 1.0 vol% MWCNT-water nanofluid is over predicted by 5.5% with a maximum deviation of 4.4%.

3.2.3 Heat transfer in the transitional flow regime

Shown in Figure 15 is the ratio of the predicted (Equation 19) to measured Nusselt numbers as a function of the transitional Reynolds numbers. The results for all three volume concentrations for the MWCNT-water nanofluids are largely outside the 10% boundary. For the 0.33 vol% MWCNT-water nanofluid, the data is over predicted by 15.6% with a maximum deviation of 84.4%, the 0.75 vol% MWCNT-water nanofluid is over predicted by 9.2% with a maximum deviation of 90.7% and the 1.0 vol% MWCNT-water nanofluid is over predicted by 12.1% with a maximum deviation of 88%.

3.3 Friction factor and pressure drop results

Shown in Figure 16 are the friction factors for the 0.33 vol%, 0.75 vol% MWCNT-water nanofluids and distilled water for the entire flow range. The results are compared with the Poiseuille equation for laminar flow and the correlation by Allen and Eckert [33] for turbulent flow.

The reason for not showing the results of the 1.0 vol% MWCNT-water nanofluid is that the pressure ports continuously became blocked and pressure readings could not be taken. This was due to the high nanoparticle concentration in the distilled water and with the pH of the solution being too close to the iso-electric point (see Figure 1), the nanoparticles agglomerated.

In the turbulent flow regime at a Reynolds number of 5 000, the friction factor for the 0.33 vol% MWCNT-water nanofluid is 0.8% higher and for the 0.75 vol% MWCNT-water nanofluid it is 2.5% lower than that of distilled water. In the laminar flow regime at a Reynolds number of 2 000, the friction factor for the 0.33 vol% MWCNT-water nanofluid is 0.7% lower and for the 0.75 vol% MWCNT-water nanofluid it is 19.7% lower than that of distilled water. The friction factors of the 0.33 vol% MWCNT-water nanofluid are very

similar to that of the water; this is most likely due to the low concentration of nanoparticles in the base fluid. As in the case of heat transfer results, the experimental friction factor data shifts to lower Reynolds numbers, this is due to the higher viscosity of the MWCNT-water nanofluids. Since MWCNT-water nanofluids exhibit a higher viscosity than water, the pressure drop of the MWCNT-water nanofluids is compared with distilled water as a function of average velocity.

Shown in Figure 17 are the measured pressure drops across the test section for the 0.33 vol%, 0.75 vol% MWCNT-water nanofluid and for distilled water for the entire flow range. The pressure drop increases with increasing average velocity. There is a slight increase in pressure drop for an increasing nanoparticle concentration. In the turbulent flow regime, $\Delta P_{nf} / \Delta P_{bf} = 1.03$ for both MWCNT-water nanofluids and in the laminar flow regime, $\Delta P_{nf} / \Delta P_{bf} = 1.1$ for the 0.33 vol% MWCNT-water nanofluid and $\Delta P_{nf} / \Delta P_{bf} = 1.2$ for the 0.75 vol% MWCNT-water nanofluid.

3.4 Performance evaluation of the MWCNT-water nanofluid

Prasher *et al.* [28] challenged the idea whether there is any benefit using nanofluids as heat transfer fluids. They considered the conservative case where $h_{nf}=h_{bf}$ and developed the design equation for nanofluids, given below

$$\frac{\Delta P_{nf}}{\Delta P_{bf}} = \left(\frac{\mu_{nf}}{\mu_{bf}}\right) \cdot \left(\frac{k_{nf}}{k_{bf}}\right)^4 \cdot \left(\frac{Nu_{nf}}{Nu_{bf}}\right)^4 \qquad (22)$$

If $\Delta P_{nf} / \Delta P_{bf} > 1$ then the nanofluid is worse as a heat transfer fluid than the base fluid, however, if it is $\Delta P_{nf} / \Delta P_{bf} < 1$, then it is a better heat transfer fluid. In the previous section where $\Delta P_{nf} / \Delta P_{bf}$ was investigated, it was shown that in the turbulent flow regime $\Delta P_{nf} / \Delta P_{bf} \approx 1$ and in the laminar flow regime, $\Delta P_{nf} / \Delta P_{bf} > 1$. Hence this indicates that in the

current study, nanofluids are better suited for the turbulent flow regime due to the shear thinning behaviour that they exhibit. In the laminar flow regime, they are worse heat transfer fluids than the base fluid, which was also indicated by the heat transfer reduction in Section 3.1. Equation 22 shows that ΔP is more sensitive to changes in thermal conductivity and Nusselt number when compared with viscosity.

For the conservative case of $Nu_{nf} = Nu_{bf}$ and desiring that ΔP_{nf} not exceed ΔP_{bf}, and substituting Equation 2 and Equation 3 into Equation 22, which then reduces to the following form

$$C_{\mu} = 4 \cdot C_{k} \qquad (23)$$

This shows that in order to have a beneficial heat transfer fluid, the increase in viscosity may not be more than four times the increase in thermal conductivity. In the current case, C_{μ} equals 60 (which is more than four times C_k), which equals 7.

4. Conclusion

Three different MWCNT-water nanofluid volume concentrations were tested for the late laminar, transition and early turbulent flow regimes. Heat transfer and pressure drop measurements were taken from a Reynolds number of 1 000 to 8 000 and compared with those of distilled water.

All three nanofluids showed enhancement when comparing the data on a *Re-Nu* graph. When comparing the data with each other at the same fluid velocity, the nanofluids showed a decrease in heat transfer coefficient when compared with water. This was due to the fact that MWCNT-water nanofluids have a larger viscosity than water and the data shifted to lower Reynolds numbers, therefore it was considered to compare the data with correlations

developed for water, which are found in literature. The correlations were modified for nanofluids and it was found that the modified correlations predicted the results to within ±10%.

Pressure drop results indicated that with increasing volume concentration, the pressure drop increases, which can be attributed to the increase in viscosity. A performance evaluation on the MWCNT-water nanofluids was done and results indicate that the increase in viscosity exceeds four times the amount of increase in thermal conductivity of the nanofluids, which is the conservative case where the heat transfer of the nanofluids equals that of the base fluid. Hence it can be concluded that the tested carbon nanofluids are not an ideal fluid for heat transfer enhancement.

Acknowledgements

The funding obtained from the NRF, TESP, University of Stellenbosch/University of Pretoria, SANERI/SANEDI, CSIR, EEDSM Hub and NAC is acknowledged and duly appreciated.

References

[1] S.M.S. Murshed, C.A.N. de Castro, M.J.V. Lourenco, M.L.M. Lopes, and F.J.V. Santos, A review of boiling and convective heat transfer with nanofluids, Renewable and Sustainable Energy Reviews, 15 (2011) 2342-2354.

[2] S.K. Das, S.U.S. Choi, and H.E. Patel, Heat transfer in nanofluids - A Review, Heat Transfer Engineering, 27 (2006) 3-19.

[3] Y. Ding, H. Alias, D. Wen, and A.R. Williams, Heat transfer of aqueous suspensions of carbon nanotubes (CNT nanofluids), International Journal of Heat and Mass Transfer, 49 (2006) 240-250.

[4] V. Trisaksri and S. Wongwises, Critical review of heat transfer characteristics of nanofluids, Renewable and Sustainable Energy Reviews, 11 (2007) 512-523.

[5] S. Kakac and A. Pramuanjaroenkij, Review of convective heat transfer enhancement with nanofluids, International Journal of Heat and Mass Transfer, 52 (2009) 3187-3196.

[6] B.C. Pak and Y.I. Cho, Hydrodynamic and heat transfer study of dispersed fluids with submicron metallic oxide particles, Experimental Heat Transfer, 11 (1998) 151-170.

[7] Q. Li and Y. Xuan, Convective heat transfer and flow characteristics of Cu-water nanofluid, Science in China, 45 (2002) 408-416.

[8] D. Wen and Y. Ding, Experimental investigation into convective heat transfer of nanofluids at the entrance region under laminar flow conditions, International Journal of Heat and Mass Transfer, 47 (2004) 5181-5188.

[9] Y. Yang, Z.G. Zhang, E.A. Grulke, W.B. Anderson, and G. Wu, Heat transfer properties of nanoparticles-in-fluid dispersions (nanofluids) in laminar flow, International Journal of Heat and Mass Transfer, 48 (2005) 1107-1116.

[10] S. Z. Heris, M. N. Esfahany, and S.Gh. Etemad, Experimental investigation of convective heat transfer of Al_2O_3/water nanofluid in circular tube, International Journal of Heat and Fluid Flow, 28 (2007) 203–210.

[11] S.M.S. Murshed, K.C. Leong, C Yang, and N.-T. Nguyen, Convective heat transfer characteristics of aqueous TiO_2 nanofluid under laminarflow conditions, International Journal of Nanoscience, 7 (2008) 325–331.

[12] P. Garg, J.L. Alvardo, C. Marsh, T.A. Carlson, D.A. Kessler, and K. Annamalai, An experimental study on the effect of ultrasonication on viscosity and heat transfer performance of multi-wall carbon nanotube-based aqueous nanofluids, International Journal of Heat and Mass Transfer, 52 (2009) 5090-5101.

[13] D. Kim, Y. Kwon, Y. Cho, C. Li, S. Cheong, Y. Hwang, J. Lee, D. Hong, and S. Moon, Convective heat transfer characteristics of nanofluids under laminar and turbulent flow conditions, Current Applied Physics, 9 (2009) 119-123.

[14] K.B. Anoop, T. Sundararajan, and S.K. Das, Effect of particle size on the convective heat transfer in nanofluid in the developing region, International Journal of Heat and Mass Transfer, 52 (2009) 2189-2195.

[15] A. Amrollahi, A.M. Rashidi, R. Lotfi, M. E. Meibodi, and K. Kashefi, Convection heat transfer of functionalized MWNT in aqueous fluids in laminar and turbulent flow at the entrance region, International Communications in Heat and Mass Transfer, 37 (2010) 717–723.

[16] Z.-H. Liu and L. Liao, Forced convective flow and heat transfer characteristics of aqueous drag-reducing fluid with carbon nanotubes added, International Journal of Thermal Sciences, 49 (2010) 2331-2338.

[17] W. Duangthongsuk and S. Wongwises, An experimental study on the heat transfer performance and pressure drop of TiO2-water nanofluids flowing under turbulent flow regime, International Journal of Heat and Mass Transfer, 53 (2010) 334-344.

[18] S. Ferrouillat, A. Bontemps, J.-P. Ribeiro, J.-A. Gruss, and O. Soriano, Hydraulic and heat transfer study of SiO2/water nanofluids in horizontal tubes with imposed wall temperature boundary conditions, International Journal of Heat and Fluid Flow, 32 (2011) 424-439.

[19] D. Liu and L. Yu, Single-phase thermal transport of nanofluids in a minichannel, Journal of Heat Transfer, 133 (2011) 1-11.

[20] J.A. Olivier and J.P. Meyer, Single-phase heat transfer and pressure drop of the cooling of water inside smooth tubes for transitional flow with different inlet geometries (RP-1280), HVAC and R, 16 (2010) 471-496.

[21] J.P. Meyer and J.A. Olivier, Transitional flow inside enhanced tubes for fully developed and developing flow with different types of inlet disturbances: Part I - Adiabatic pressure drop, International Journal for Heat and Mass Transfer, 54 (2011) 1587-1598.

[22] J.P. Meyer and J.A. Olivier, Transitional flow inside enhanced tubes for fully developed and developing flow with different types of inlet disturbances: Part II - Heat transfer, International Journal for Heat and Mass Transfer, 54 (2011) 1598-1607.

[23] S.W. Lee, S.D. Park, S. Kang, I.C. Bang, and J.H. Kim, Investigation of viscosity and thermal conductivity of SiC nanofluids for heat transfer applications, International Journal of Heat and Mass Transfer, 54 (2011) 433-438.

[24] H. Xie, H. Lee, W. Youn, and M. Choi, Nanofluids containing multiwalled carbon nanotubes and their enhanced thermal conductivities, Journal of Applied Physics, 94 (2003) 4967-4971.

[25] C.O. Popiel and J. Wojtkowiak, Simple formulas for thermophysical properties of liquid water for heat transfer calculations, Heat Transfer Engineering, 19 (1998) 87-101.

[26] R. Prasher, P.E. Phelan, and P. Bhattacharya, Effect of aggregation kinetics on the thermal conductivity of nanoscale colloidal solutions (Nanofluid), Nano Letters, 6 (2006) 1529-1534.

[27] P. Keblinski, S.R. Phillpot, S.U.S. Choi, and J.A. Eastman, Mechanisms of heat flow in suspensions of nano-sized particles (nanofluids), International Journal of Heat and Mass Transfer, 45 (2002) 855-863.

[28] R. Prasher, D. Song, J. Wang, and P.E. Phelan, Measurements of nanofluids viscosity and its implications for thermal applications, Applied Physics Letters, 89 (2006) 1-3.

[29] P.C. Hiemenz, *Principles of colloid and surface chemistry*, 2nd ed.: Marcel Dekker, Inc., 1986, vol. 9.

[30] S.I. Abu-Eishah, Correlations for the thermal conductivity of metals as a function of temperature, International Journal of Heat and Mass Transfer, 22 (2001) 1855-1868.

[31] Y.A. Cengel, *Heat and mass transfer - A practical approach*, 2nd ed.: McGraw Hill, 2006.

[32] R.J. Moffat, Describing the uncertainties in experimental results, Experimental Thermal and Fluid Science, 1 (1988) 3-17.

[33] R.W. Allen and E.R.G. Eckert, Friction and heat-transfer measurements to turbulent pipe flow of water (Pr = 7 and 8) at uniform wall heat flux, Journal of Heat Transfer, 86 (1964) 301-310.

[34] B. Shome and M.K. Jensen, Mixed convection laminar flow and heat transfer of liquids in isothermal horizontal circular ducts, International Journal of Heat and Mass Transfer, 38 (1995) 1945-1956.

[35] L.-M. Tam and A.J. Ghajar, Effect of inlet geometry and heating on the fully developed friction factor in the transition region of a horizontal tube, Experimental Thermal and Fluid Science, 15 (1997) 52-64.

[36] B. Metais and E.R.G. Eckert, Forced, Mixed and Free Convection Regimes, Transactions of the ASME Journal of Heat Transfer, 10 (1964) 295-296.

[37] A.J. Ghajar and L.-M. Tam, Flow regime map for a horizontal pipe with uniform wall heat flux and three inlet configurations, Experimental Thermal and Fluid Science, 10 (1995) 287-297.

[38] A.J. Ghajar and L.-M. Tam, Heat transfer measurements and correlations in the transition region for a circular tube with three different inlet configurations, 8 (1994) 79-90.

[39] Y. Xuan and Q. Li, Investigation on convective heat transfer and flow features of nanofluids, Journal of Heat Transfer, 125 (2003) 151-155.

[40] W. Yu, D.M. France, D.S. Smith, D. Singh, E.V. Timofeeva, and J.L. Routbort, Heat transfer to silicon carbide/water nanofluid, International Journal of Heat and Mass Transfer, 52 (2009) 3606-3612.

[41] W. Williams, J. Buongiorno, and L.-W. Hu, Experimental investigation of turbulent convective heat transfer and pressure loss of alumina/water and zirconia/water nanoparticle colloids (nanofluids) in horizontal tubes, Journal of Heat Transfer, 130 (2008) 042412-7pages.

[42] G.H. Ko, K. Heo, K. Lee, D.S. Kim, C. Kim, Y. Sohn, and M. Choi, An experimental study on the pressure drop of nanofluids containing carbon nanotubes in a horizontal tube, International Heat and Mass Transfer, 50 (2007) 4749-4753.

[43] L.-M. Tam and A.J. Ghajar, The unusual behaviour of local heat transfer coefficient in a circular tube with a bell-mouth inlet, Experimental Thermal and Fluid Science, 16 (1998) 187-194.

[44] Y. Xuan and W. Roetzel, Conceptions for heat transfer correlation of nanofluids, International Journal of Heat and Mass Transfer, 43 (2000) 3701-3707.

[45] X.Q. Wang and A.S. Mujumdar, Heat transfer characteristics of nanofluids: A review, International Journal of Thermal Sciences, 46 1-19.

[46] L Liao and Z.-H. Zhen-Hua Liu, Forced convective flow drag and heat transfer characteristics of carbon nanotube suspensions in a horizontal small tube, Heat Mass Transfer, 45 (2009) 1129–1136.

List of Figures

Figure 1 Measured pH of the MWCNT-water nanofluid compared with that of GA-water mixture and distilled water

Figure 2 Measured relative thermal conductivity of the MWCNT-water nanofluid as a function of the volume concentration compared to Prasher *et al.* [28] (Note: At a concentration of 0%, all measurement points are lying on top of each other)

Figure 3 Relative viscosity of the MWCNT-water nanofluid as a function of the volume concentration compared to theory (Note: At a concentration of 0%, all measurement points are lying on top of each other)

Figure 4 Schematic representation of the experimental set-up

Figure 5 Schematic representation of the test section

Figure 6 Validation of the water adiabatic friction factor results as a function of Reynolds number

Figure 7 Water diabatic friction factors results as a function of the Reynolds number

Figure 8 Water laminar-turbulent heat transfer results on the flow regime map of Ghajar and Tam [37]

Figure 9 Smooth tube heat transfer results compared with the work of Ghajar and Tam [38] for water

Figure 10 Nusselt number results of different concentrations of MWCNT-water nanofluids as a function of average Reynolds numbers

Figure 11 Heat transfer coefficient results of different concentrations of MWCNT-water nanofluids as a function of average velocity

Figure 12 Local heat transfer coefficients for different concentrations of MWCNT-water nanofluids as a function of axial distance from the inlet compared with water at a Reynolds number of 2 000

Figure 13 Ratio of the predicted [38] to measured Nusselt numbers as a function of the laminar Reynolds number

Figure 14 Ratio of the predicted [38] to measured Nusselt numbers as a function of the turbulent Reynolds number

Figure 15 Ratio of the predicted [38] to measured Nusselt numbers as a function of the transitional Reynolds numbers

Figure 16 Friction factor of the MWCNT-water nanofluids compared with distilled water

Figure 17 Pressure drop of the MWCNT-water nanofluids compared with water

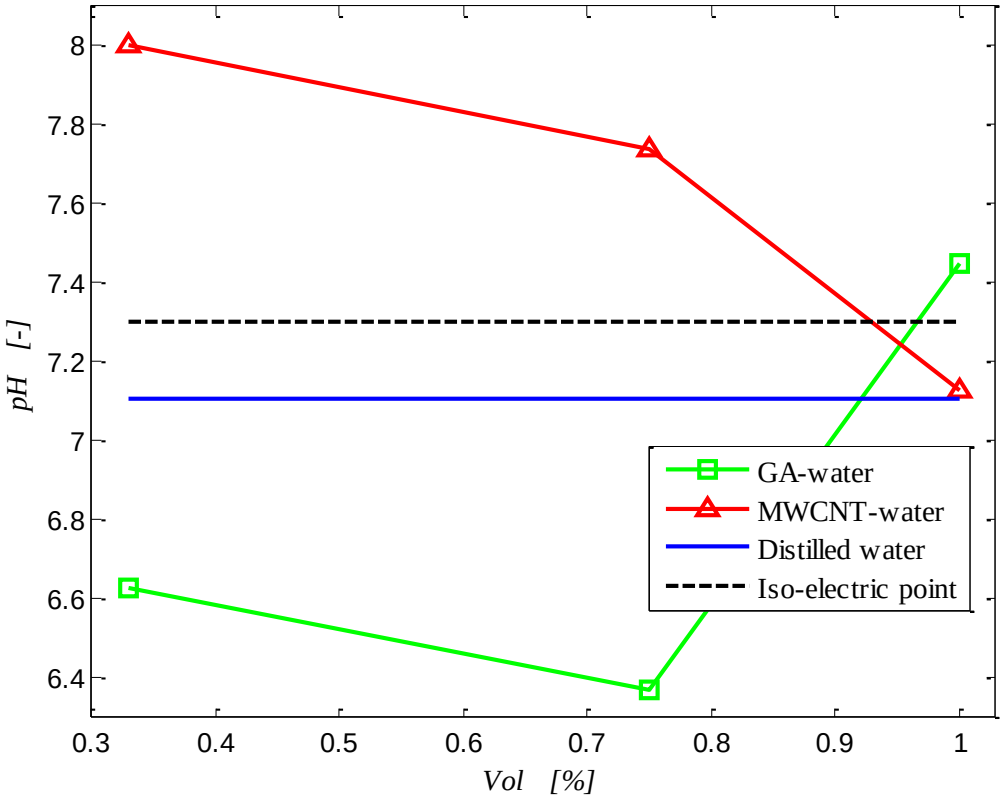
8
7.8
7.6
7.4
7.2
7
6.8
6.6
6.4
pH [-]
0.3
0.4
0.5
0.6
0.7
0.8
0.9
1
Vol [%]
GA-water
MWCNT-water
Distilled water
Iso-electric point

Figure 1

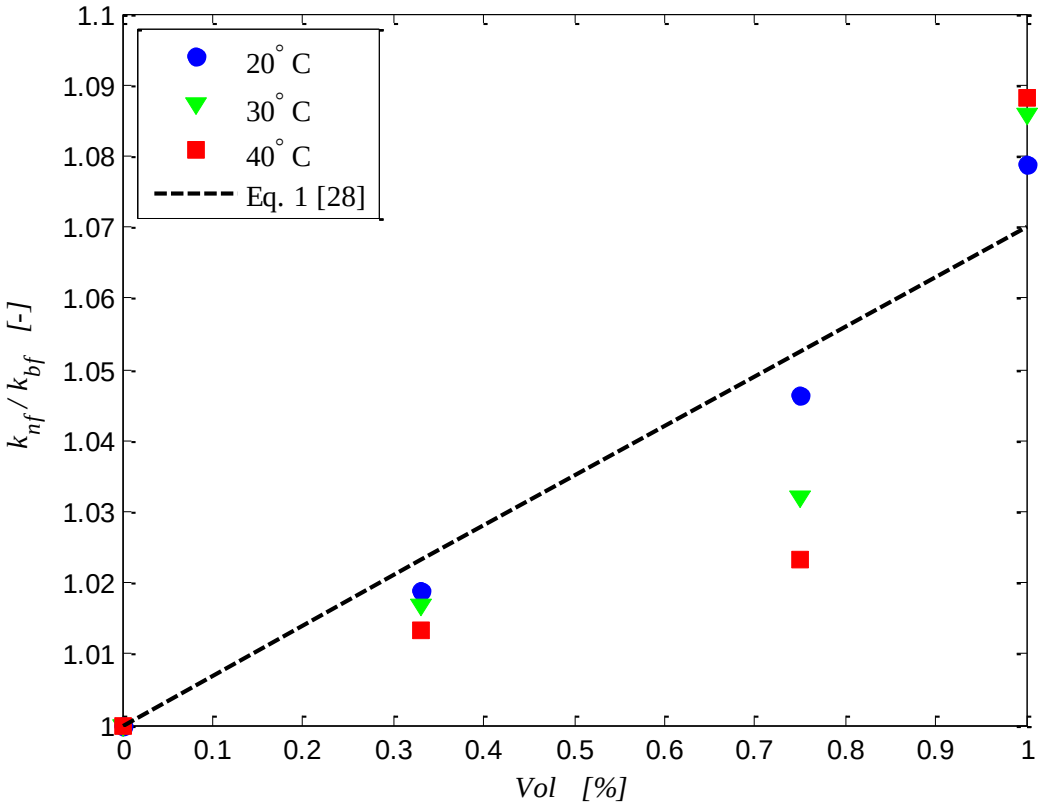
20° C
30° C
40° C
Eq. 1 [28]
k_{nf}/k_{bf} [-]
Vol [%]
1.1
1.09
1.08
1.07
1.06
1.05
1.04
1.03
1.02
1.01
1
0
0.1
0.2
0.3
0.4
0.5
0.6
0.7
0.8
0.9
1

Figure 2

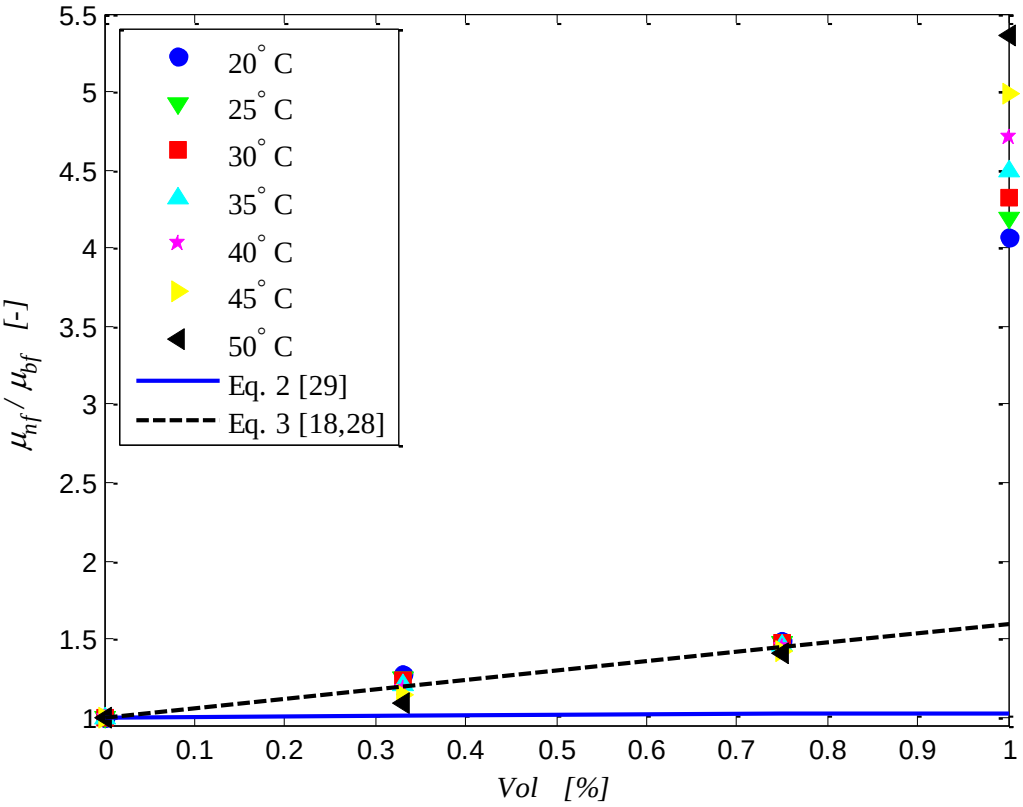
20° C
25° C
30° C
35° C
40° C
45° C
50° C
Eq. 2 [29]
Eq. 3 [18,28]
μ_{hf}/μ_{bf} [-]
Vol [%]
5.5
5
4.5
4
3.5
3
2.5
2
1.5
1
0
0.1
0.2
0.3
0.4
0.5
0.6
0.7
0.8
0.9
1

Figure 3

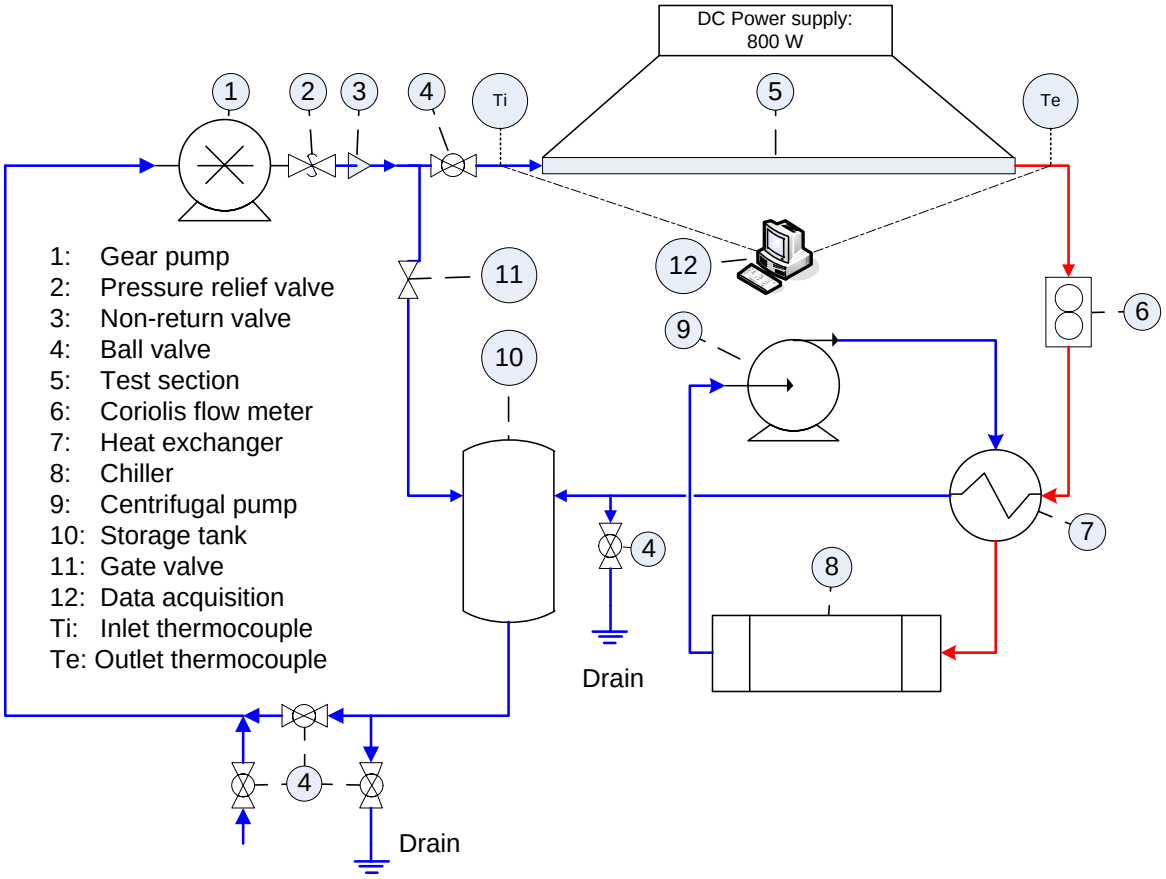
DC Power supply:
800 W
1: Gear pump
2: Pressure relief valve
3: Non-return valve
4: Ball valve
5: Test section
6: Coriolis flow meter
7: Heat exchanger
8: Chiller
9: Centrifugal pump
10: Storage tank
11: Gate valve
12: Data acquisition
Ti: Inlet thermocouple
Te: Outlet thermocouple
Drain
Drain

Figure 4

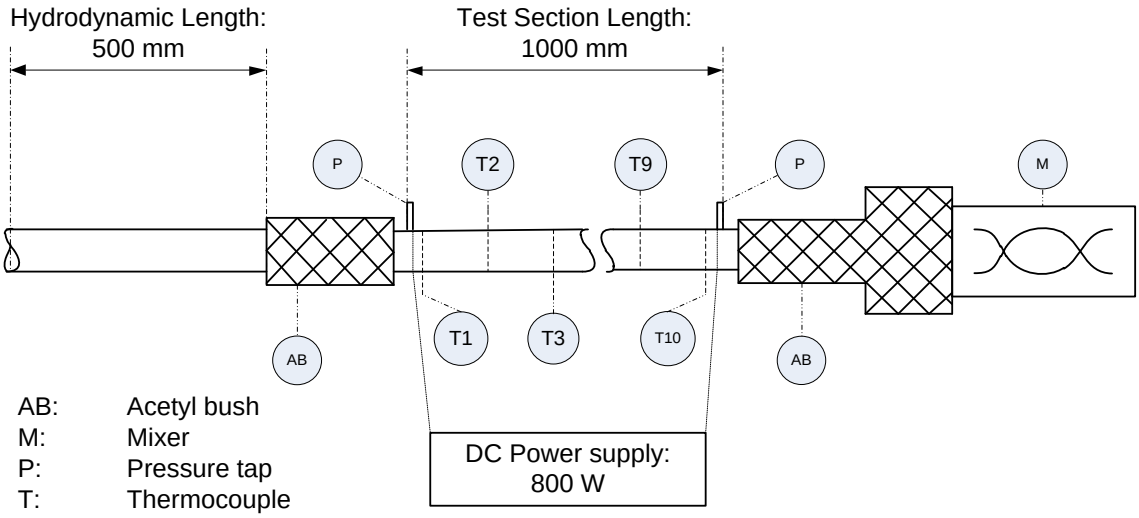
Hydrodynamic Length:
500 mm
Test Section Length:
1000 mm
P
T2
T9
P
M
AB
T1
T3
T10
AB
AB: Acetyl bush
M: Mixer
P: Pressure tap
T: Thermocouple
DC Power supply:
800 W

Figure 5

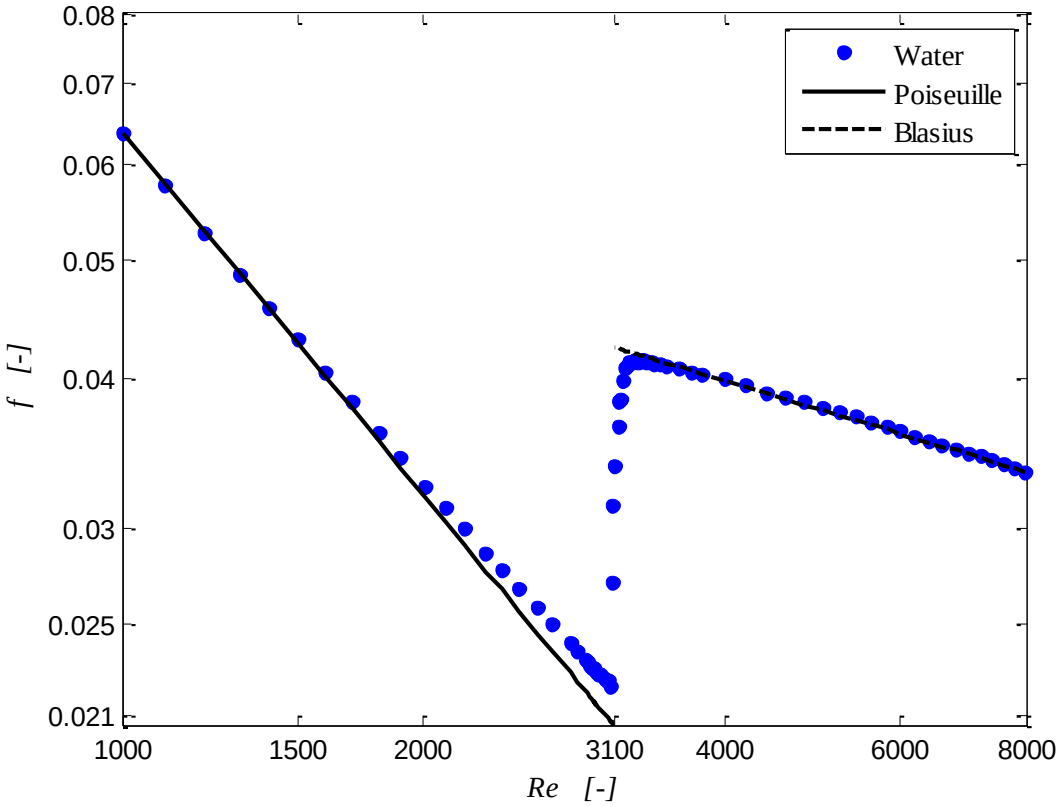
0.08
0.07
0.06
0.05
0.04
0.03
0.025
0.021
f [-]
1000
1500
2000
3100
4000
6000
8000
Re [-]
Water
Poiseuille
Blasius

Figure 6

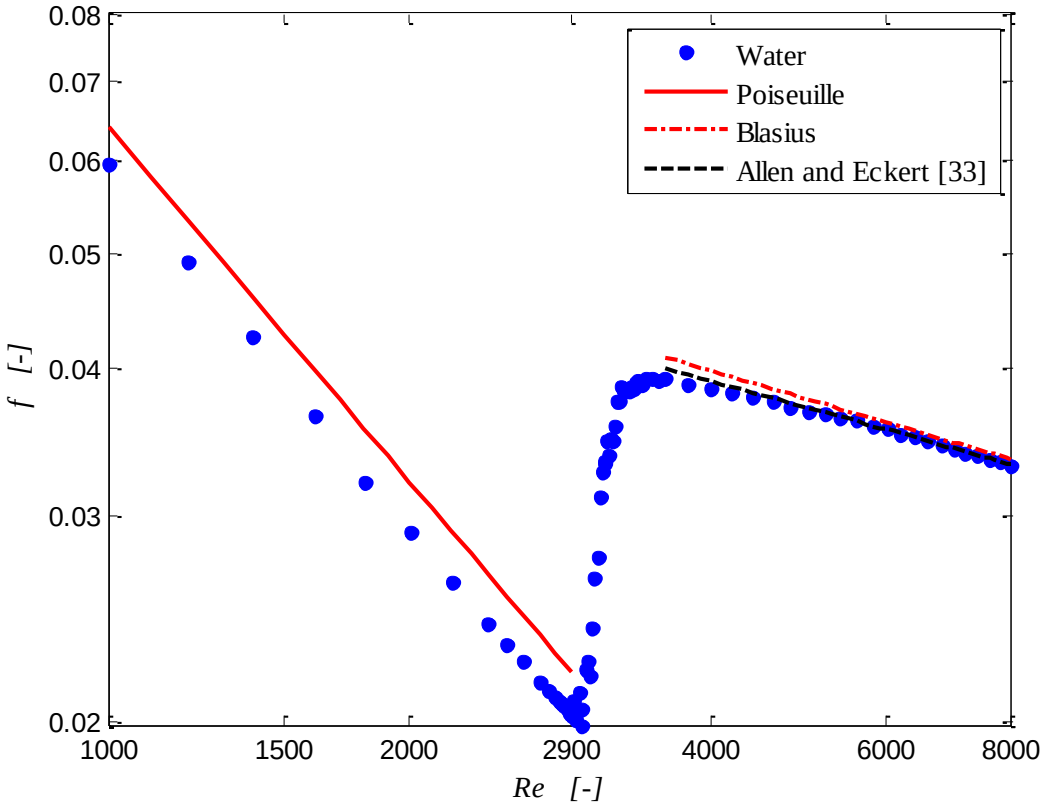
0.08
0.07
0.06
0.05
0.04
0.03
0.02
f [-]
1000
1500
2000
2900
4000
6000
8000
Re [-]
Water
Poiseuille
Blasius
Allen and Eckert [33]

Figure 7

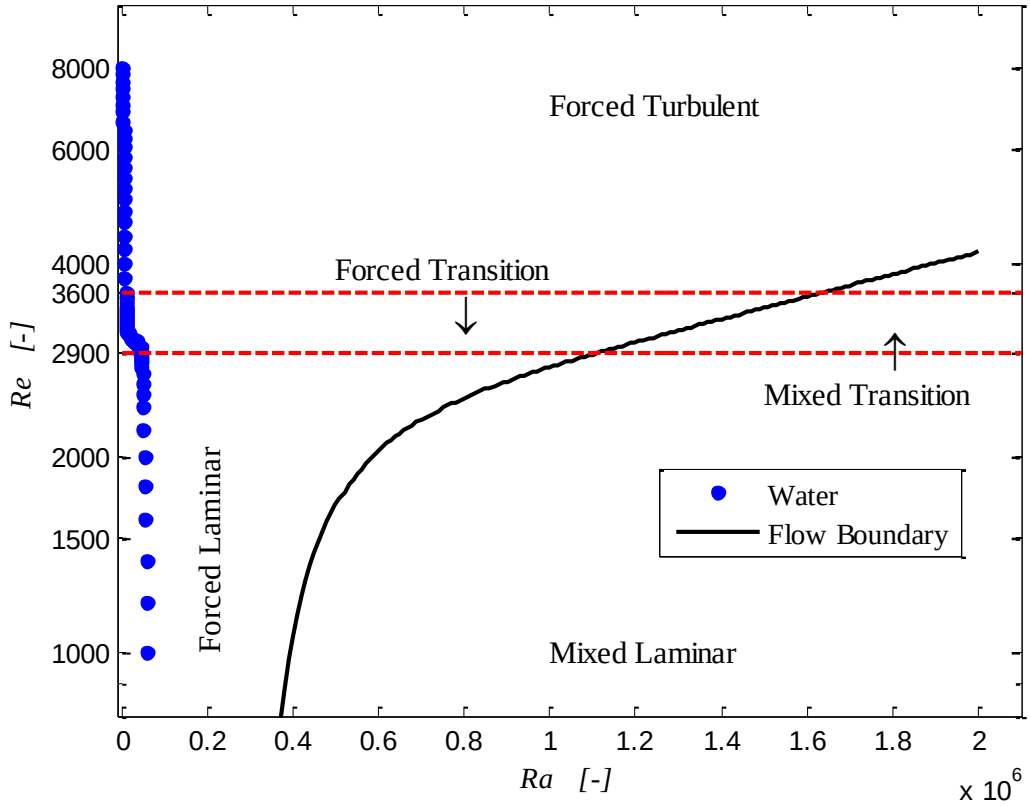
8000
6000
4000
3600
2900
2000
1500
1000
Re [-]
Forced Turbulent
Forced Transition
Mixed Transition
Forced Laminar
Mixed Laminar
Water
Flow Boundary
0
0.2
0.4
0.6
0.8
1
1.2
1.4
1.6
1.8
2
Ra [-]
x 10^6

Figure 8

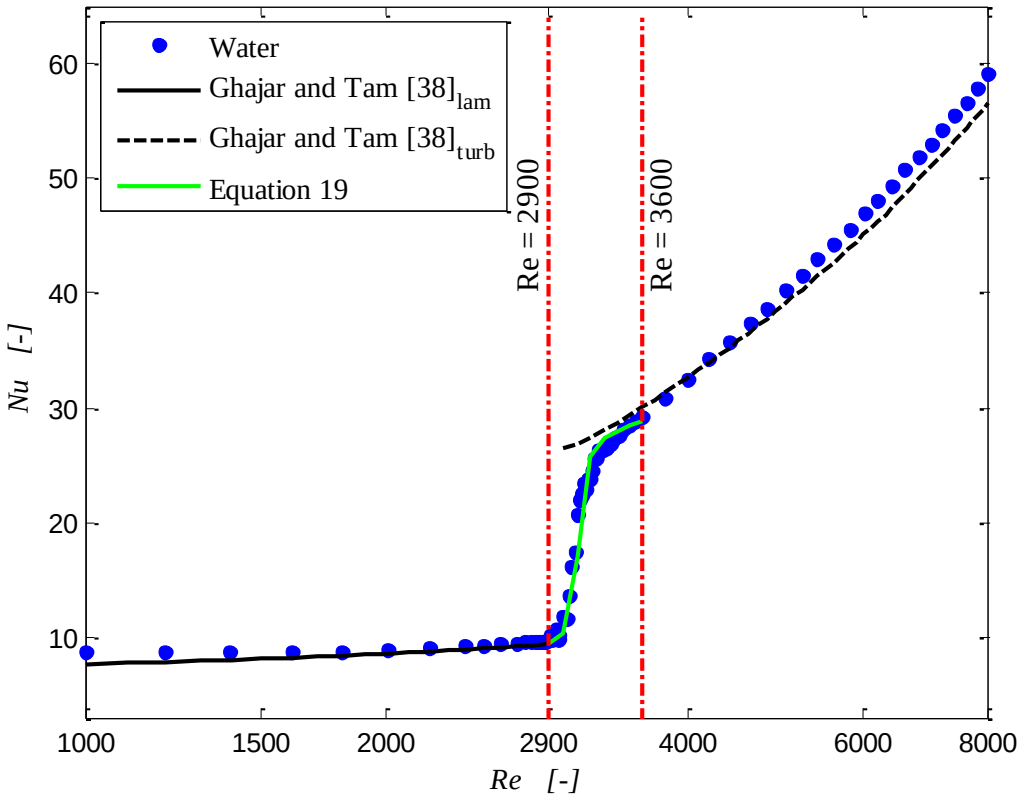
Water
Ghajar and Tam [38]lam
Ghajar and Tam [38]turb
Equation 19
Re = 2900
Re = 3600
Nu [-]
Re [-]
60
50
40
30
20
10
1000
1500
2000
2900
4000
6000
8000

Figure 9

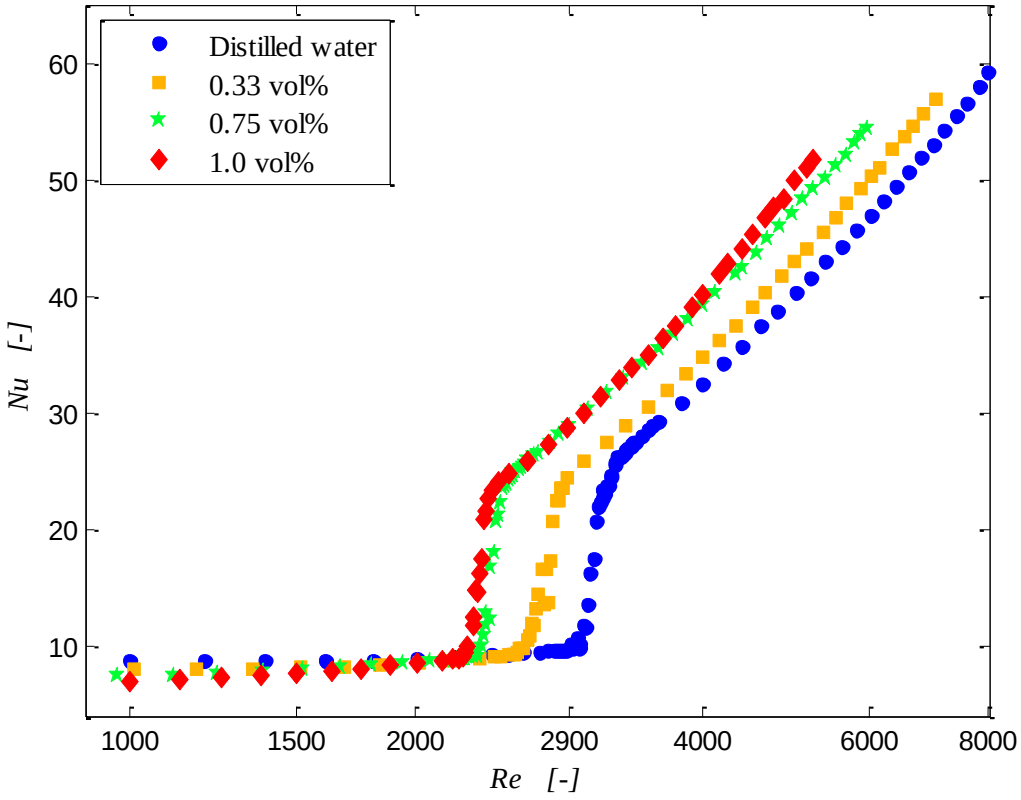
Distilled water
0.33 vol%
0.75 vol%
1.0 vol%
Nu [-]
Re [-]
60
50
40
30
20
10
1000
1500
2000
2900
4000
6000
8000

Figure 10

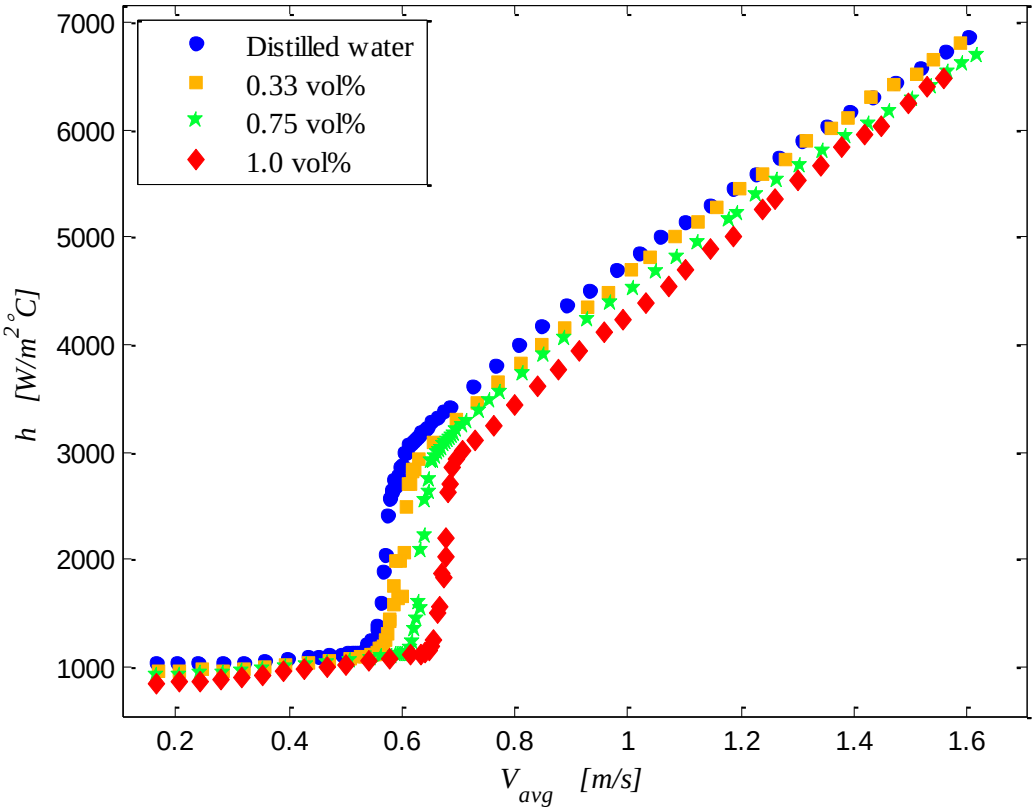
Distilled water
0.33 vol%
0.75 vol%
1.0 vol%
7000
6000
5000
4000
3000
2000
1000
h [W/m2°C]
0.2
0.4
0.6
0.8
1
1.2
1.4
1.6
Vavg [m/s]

Figure 11

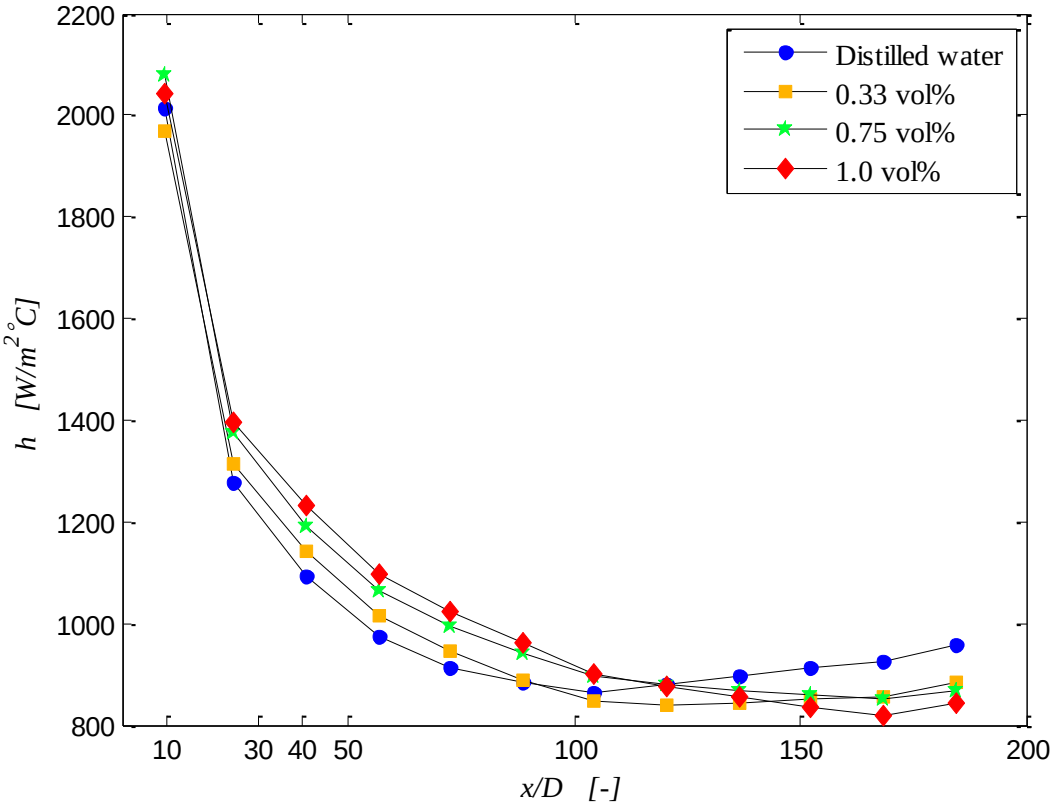
2200
2000
1800
1600
1400
1200
1000
800
h [W/m2°C]
10
30
40
50
100
150
200
x/D [-]
Distilled water
0.33 vol%
0.75 vol%
1.0 vol%

Figure 12

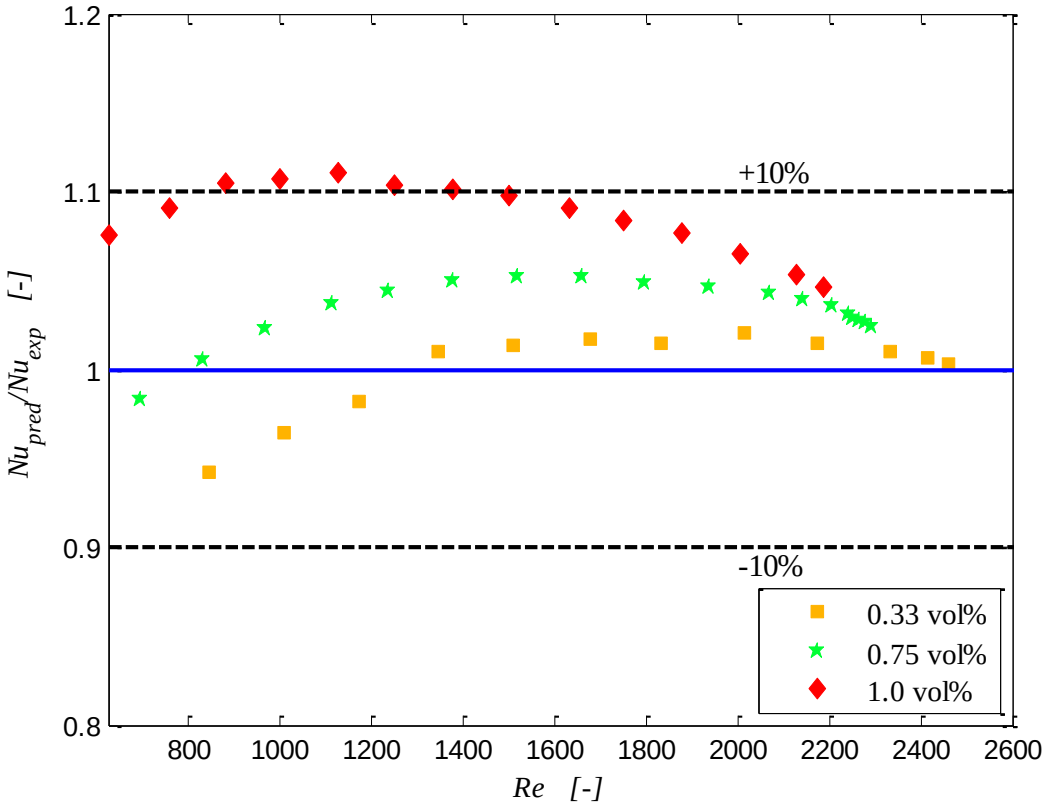
1.2
1.1
1
0.9
0.8
+10%
-10%
0.33 vol%
0.75 vol%
1.0 vol%
800
1000
1200
1400
1600
1800
2000
2200
2400
2600
Re [-]
Nu_pred/Nu_exp [-]

Figure 13

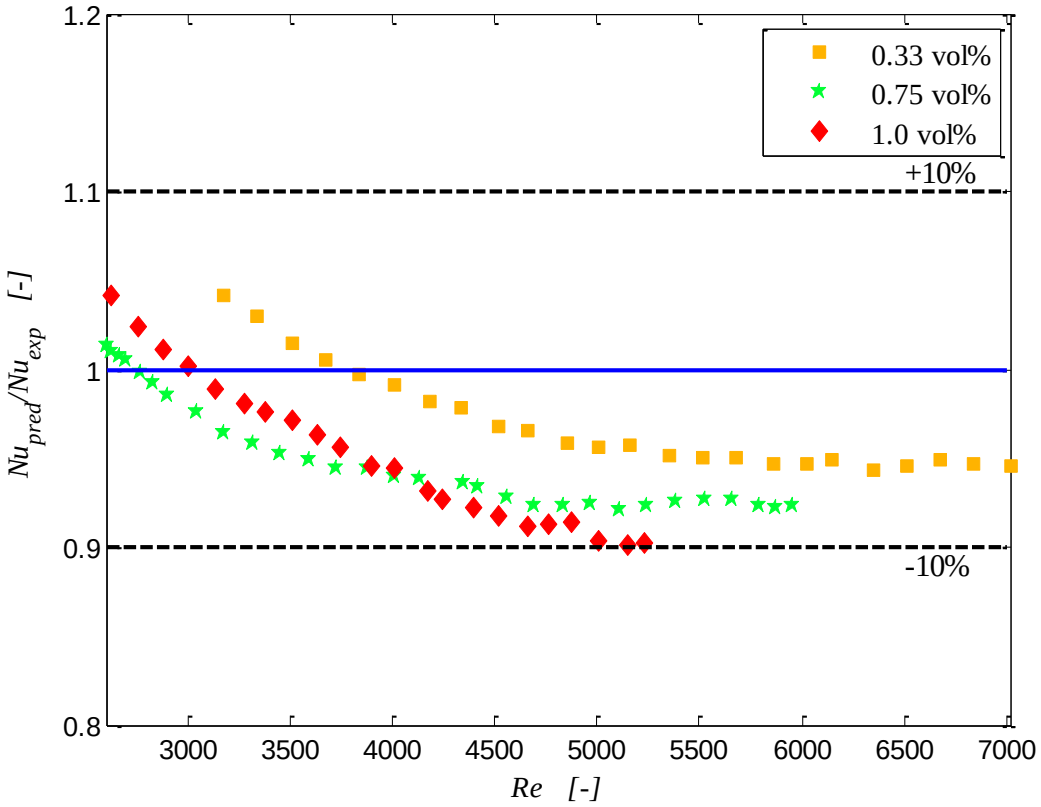
1.2
1.1
1
0.9
0.8
3000
3500
4000
4500
5000
5500
6000
6500
7000
0.33 vol%
0.75 vol%
1.0 vol%
+10%
-10%
Nu_{pred}/Nu_{exp} [-]
Re [-]

Figure 14

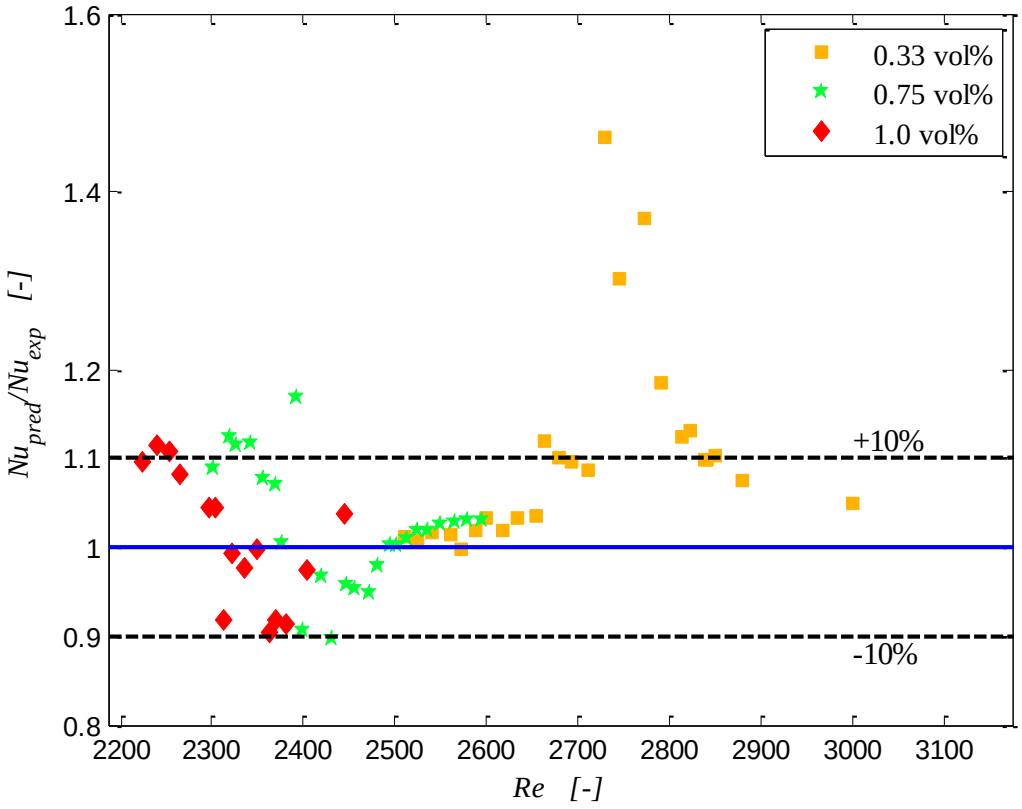
0.33 vol%
0.75 vol%
1.0 vol%
+10%
-10%
1.6
1.4
1.2
1.1
1
0.9
0.8
2200
2300
2400
2500
2600
2700
2800
2900
3000
3100
Nu_pred/Nu_exp [-]
Re [-]

Figure 15

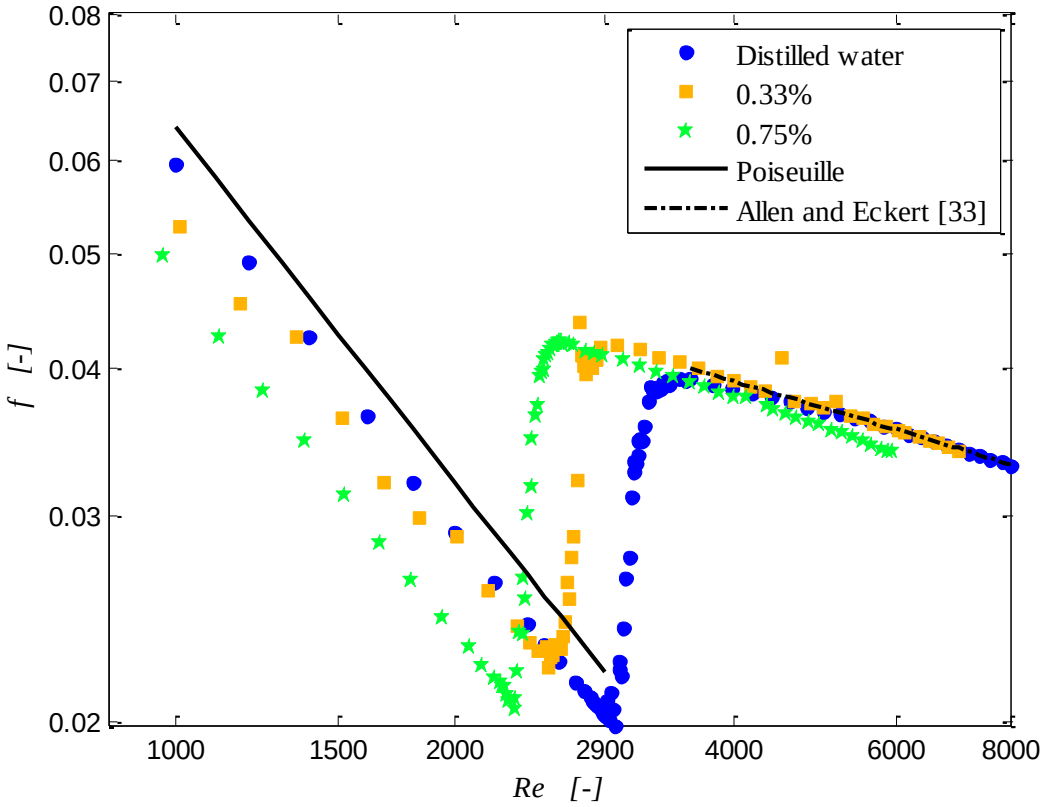
0.08
0.07
0.06
0.05
0.04
0.03
0.02
f [-]
1000
1500
2000
2900
4000
6000
8000
Re [-]
Distilled water
0.33%
0.75%
Poiseuille
Allen and Eckert [33]

Figure 16

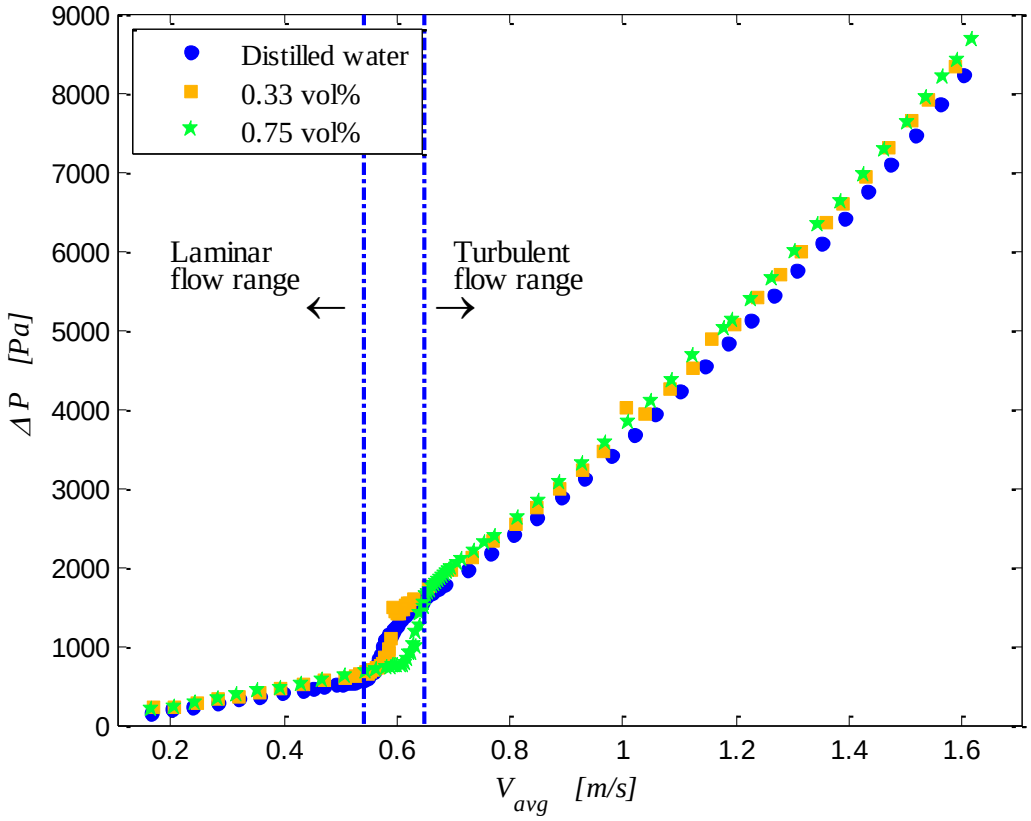
Distilled water
0.33 vol%
0.75 vol%
Laminar
flow range
Turbulent
flow range
ΔP [Pa]
V_avg [m/s]
9000
8000
7000
6000
5000
4000
3000
2000
1000
0
0.2
0.4
0.6
0.8
1
1.2
1.4
1.6

Figure 17

List of Tables

Table 1: Comparison of previous work in terms of flow range, type of nanofluid and enhancement

Table 2: Ranges and accuracies of instruments

Table 3: Uncertainties of experimental parameters

Table 1: Comparison of previous work in terms of flow range, type of nanofluid and enhancement

Author	Flow Range	Nanofluid	Result
Pak and Cho [6]	Turbulent	γ-Al_2O_3-water TiO_2-water	45% enhancement 75% enhancement
Li and Xuan [7]	Laminar and turbulent	Cu-water	60% enhancement
Wen and Ding [8]	Laminar	γ-Al_2O_3-water	45% enhancement for developing flow
Yang *et al.* [9]	Laminar	Graphite-water	22% enhancement at 50°C 15% enhancement at 70°C
Ding *et al.* [3]	Laminar	MWCNT-water	350% enhancement at the entrance region
Murshed *et al.* [11]	Laminar	TiO_2-water	12% and 14% enhancement at the entrance region
Garg *et al.* [12]	Laminar	MWCNT-water	32% enhancement
Kim *et al.* [13]	Laminar and turbulent	γ-Al_2O_3-water A/C-water	14% enhancement, laminar 7% enhancement, laminar
Anoop *et al.* [14]	Laminar	γ-Al_2O_3-water	25% enhancement for 45 nm 11% enhancement for 150 nm
Amrollahi *et al.* [15]	Laminar and turbulent	Functionalized MWCNT-water	25% enhancement in laminar flow and 5-25% enhancement in turbulent flow
Liu and Liao [16]	Turbulent	aqueous drag-reducing fluid with CNT	40% enhancement
Duangthongsuk and Wongwises [17]	Turbulent	TiO_2-water	26% enhancement for 1 vol% -14% enhancement for 2 vol%
Ferrouillat *et al.* [18]	Turbulent	SiO_2-water	50% enhancement for 18.9 vol%

Table 2: Ranges and accuracies of instruments

Instrument	Range	Uncertainty
Thermocouple		
Inlet/Outlet	-200 to 350 °C	0.1 °C
Station	-200 to 350 °C	0.1 °C
Coriolis flow meter	0 - 0.07 kg/s	0.1%
Pressure transducer	0 – 17 kPa	0.16 %
Power supply	0 – 320 V	0.33 V
	0 – 12.5 A	0.04 A

Table 3: Uncertainties of experimental parameters

Property	Low Re	High Re
$\dot{m}$	1.99 %	0.2 %
T_m	0.11 °C	0.1 °C
$\dot{q}_{in}$	3.49 %	3.49 %
h	1.35 %	1.35 %
Nu	2.45 %	3.19 %
Re	2.26 %	1.09 %
ΔP	17.5 %	0.3 %
f	18 %	2.0 %